



Structural Health Monitoring of Multi-Storey Frame Structures using Piezoelectric Incompatibility Filters: Theory and Numerical Verification

Michael Krommer¹, Markus Zellhofer², Hans Irschik³

¹Institute of Technical Mechanics, Johannes Kepler University Linz, Altenberger Straße 69, A-4040 Linz, Austria, Email: michael.krommer@jku.at

²HBLA Francisco Josephinum Wieselburg, Schloss Weinzierl 1, A-3250 Wieselburg, Austria, Email: markus.zellhofer@josephinum.at

³Institute of Technical Mechanics, Johannes Kepler University Linz, Altenberger Straße 69, A-4040 Linz, Austria, Email: hans.irschik@jku.at

Received April 13 2020; Revised June 13 2020; Accepted for publication June 13 2020.

Corresponding author: Michael Krommer (michael.krommer@jku.at)

© 2021 Published by Shahid Chamran University of Ahvaz

Abstract. In the present paper we develop a novel method for structural health monitoring of multi-storey frame structures with the capability to detect and localise local damage. The method uses so-called spatial incompatibility filters, which are continuously distributed strain-type sensors only sensitive to incompatibilities. In the first part of the paper the concept of incompatibility filters is introduced for multi-storey frame structures and it is shown how these filters can be used to detect and localise local cracks in frame structures. In the second part of the paper we study the use of incompatibility filters put into practice by piezoelectric sensor networks for structural health monitoring of a three-storey frame structure. The design of the piezoelectric sensor network is based on an analytical analysis of the frame structure within the framework of the method developed in the first part of the paper and a numerical verification using three-dimensional Finite Elements completes the paper.

Keywords: Structural Health Monitoring, Frame Structures, Incompatibility Filters, Damage Detection and Localisation, Piezoelectric Sensor Networks, Numerical Verification.

1. Introduction

Smart structure technology has been considered a key technology for the design of so-called intelligent, civil, mechanical and aerospace structures since the end of the last millennium. For early reviews see [1, 2] and challenges and opportunities as envisioned at the beginning of this millennium were discussed in [3, 4]. The field of smart structures requires a multi-disciplinary approach, which involves coupled multi-field modeling of the structure, the communication between the structure and a controller (enabled by means of suitable sensor and actuator systems), the structural integration of the smart system and its practical implementation. A key aspect within these topics is the proper functioning of the communication between the structure and the controller; this communication has been denoted as control-structure interaction in the literature, see [5]. In particular, sensors are responsible for converting mechanical entities into information about the state of the structure, which must be interpreted and processed by the controller to control the structure. Strategic issues concerning sensor design were discussed in [3] and frontiers in sensors/sensor systems were pointed out in [6]. Particular fields of application of smart structures that have always gained high attention by numerous researchers are vibration monitoring, active vibration control and noise reduction; see e.g. [7, 8, 9, 10] among many others.

One crucial point in the design of a smart structure is the spatial distribution of sensors to obtain relevant information, both for monitoring and control, as the structures under consideration are typically continuous structures [5]. Hence, the spatial distribution of the smart sensing system ideally is continuous as well, resulting into so-called continuously distributed sensors. A prominent example are continuously distributed strain-type sensors, which produce a signal that represents a weighted integral over the strain a body is suffering. Such distributed sensor systems have been studied for some time and are also known under the notion of a spatial filter as they filter certain spatial information; e.g. the celebrated concept of modal filters, which filter the modal content of only one vibration mode of a structure [11], displacement filters, which filter the displacement of a specific point in a specific direction [12] or volume displacement filters [13]. Besides modal, displacement and volume filters, the concept of incompatibility filters, which filter the incompatible part of the strain tensor has been introduced in [14]. In earlier works such filters have also been denoted as nilpotent sensors [15]; their signal is trivial as long as the strain is compatible. In general, spatial filters are widely used in structural control [16] and vibration based structural health monitoring and damage detection [17, 18, 19, 20, 21]. Concerning our own previous work on the use of continuously distributed strain-type sensors in structural mechanics we refer to [22].

It has been mentioned in the literature that spatial filters can be put into practice either by continuously distributed sensors or by arrays/networks of dense sensors; in both cases the use of piezoelectric sensors is a popular choice. On the one hand, because piezoelectric sensors can actually be put into practice as continuously distributed sensors [23], and on the other hand, because sensor networks can be easily implemented by means of piezoelectric patches (see e.g. [24] for the application of piezoelectric transducers for structural health monitoring). In the latter case of sensor networks the distribution is achieved by a proper placement and



weight (intensity) assignment to the individual members of the network in order to approximate the spatially distributed sensor. In [25] a review on corresponding opportunities and challenges in smart sensor technology was presented; in particular with respect to densely instrumented arrays of sensors that will be required for the next generation of health monitoring and control systems. One of the critical issues mentioned in [25] is the lack of a computational framework on which to build new strategies for realizing massively distributed smart sensors. We seek to answer this question by designing a network of piezoelectric sensors approximating a corresponding continuously distributed strain-type sensor using a simple method based on statically equivalent force systems. For a review on alternative methods to optimally place piezoelectric sensors and actuators see [26] and for a level set based method to design distributed modal sensors we refer to [27].

In the present paper, we study a three-storey frame structure with attached piezoelectric patches; a sensor network constituted by these individual patches is designed to monitor the structural health of the frame structure. In particular, we focus on incompatibility filters as a novel concept in structural health monitoring, by means of which we combine the advantages of spatial filtering techniques for structural health monitoring with nondestructive defect detection techniques based on the principle of strain compatibility, see [28, 29]. Concerning our own previous work on this subject we refer to [30] for the monitoring of the relative horizontal floor displacements using displacement filters and to [31, 32] for health monitoring using incompatibility filters. The novelty of this contribution is that we use the piezoelectric sensor network as a health monitoring system, which can detect and localise local damage, but is also capable of directly monitoring the damage of a damaged frame structure. Moreover, the results, which are based on beam theory are numerically verified using three-dimensional Finite Elements. Concerning health monitoring we focus on damage, which can be modeled as an intermediate hinge with a residual stiffness in case beam theory is used. Such a modeling is known to mimic a crack with a certain relative depth; see e.g. [33] for a discussion of different approaches concerning the computation of the residual stiffness. In the Finite Element verification the crack is simply modeled as an imperfect connection between two surfaces, which both represent the same cross section.

2. Design of nilpotent strain-type sensors in multi-storey frame structures

In this section we discuss the design of continuously distributed strain-type sensors for the monitoring of multi-storey frame structures; hence, the design of spatial filters for frame structures. For the sake of brevity, we restrict to two-dimensional frame structures that deform in their own plane; our subsequent formulations however can be extended to more complex structural systems with relative ease. In particular, we are interested in designing spatial filters, which measure a trivial signal independent from the actual motion of the structure. We study multi-storey frame structures made of flexible vertical sidewalls that undergo a plane bending motion, where the horizontal floors are assumed to be rigid. The sidewalls, which we model as Bernoulli-Euler beams, are rigidly connected to the floors; the motion of the latter we assume to be only horizontal. At the lowest storey the sidewalls are clamped to the ground. A sketch of a three-storey frame structure is shown in Fig. 1, in which a front view is shown in the left figure and a side view in the right figure; in the latter side view, we also show piezoelectric patches attached to the flexible sidewalls, which will be used later on to put spatial filters into practice in a case study concerned with such a three-storey frame structure. Mathematically, we introduce a spatial filter as a continuously distributed strain-type sensor, the signal of which can be computed

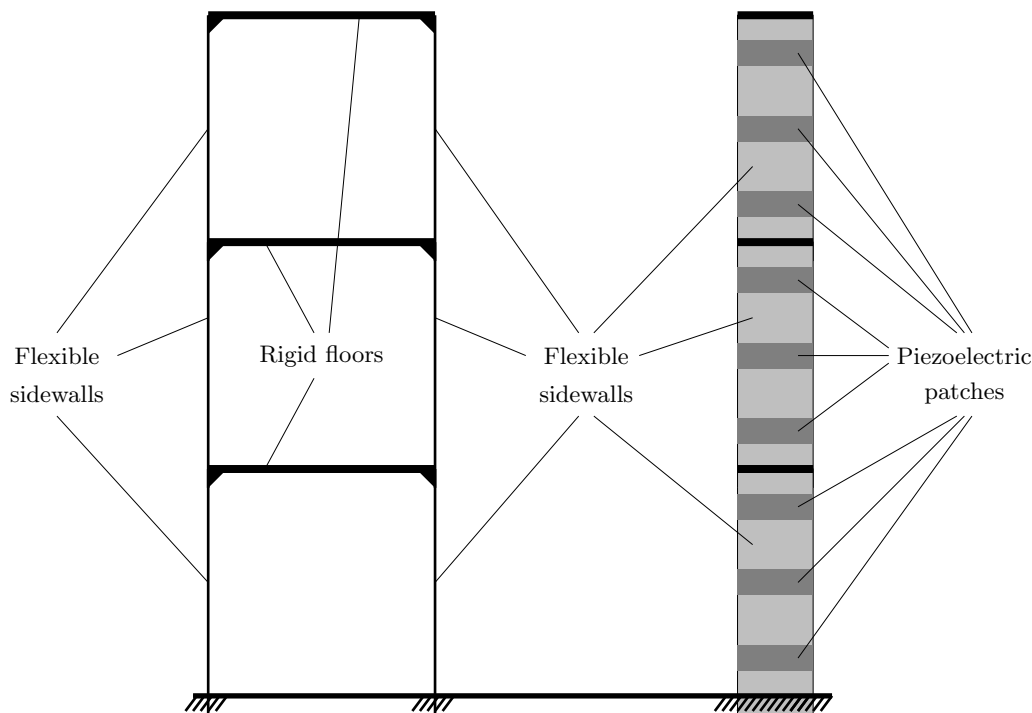


Fig. 1. Sketch of a three-storey frame structure: Front view (left) and side view (right)

from the strain the structure suffers in all its flexible parts. In our case this means within the flexible sidewalls. Assuming the structure to have n storeys, the signal of such a sensor is

$$y(t) = - \sum_{i=1}^n \left(\int_0^{h_i} S_{iL}(x_{iL}) \frac{\partial^2 w_{iL}(x_{iL})}{\partial x_{iL}^2} dx_{iL} + \int_0^{h_i} S_{iR}(x_{iR}) \frac{\partial^2 w_{iR}(x_{iR})}{\partial x_{iR}^2} dx_{iR} \right). \quad (1)$$



In Eq. (1) the subscripts L and R refer to the left and right sidewalls, h_i is the height of the i -th storey, $x_{i(L,R)}$ are local axial coordinates, $w_{i(L,R)}$ is the horizontal displacement / deflection of the flexible sidewalls and $S_{i(L,R)}$ the so-called sensor shape functions, which define the continuous distribution of the spatial filter. To obtain a non-dimensional sensor signal, the sensor shape functions are assumed to be non-dimensional $[S_{i(L,R)}] = 1$. As we are within the Bernoulli-Euler beam theory, strain refers to the negative linearized curvature in each sidewall, $\kappa_{i(L,R)} = -\partial^2 w_{i(L,R)}(x_{i(L,R)}) / \partial x_{i(L,R)}^2$. The sensor design problem we wish to solve can be stated as follows:

Find nontrivial $S_{iL}(x_{iL})$ and $S_{iR}(x_{iR})$ for all sidewalls such that the combined sensor output in Eq. (1) measures a trivial signal.

The nontrivial sensor shape functions $S_{iL}(x_{iL})$ and $S_{iR}(x_{iR})$ are denoted as *nilpotent*; they exist in redundant structures only. In this paper we will discuss the use of nilpotent sensor shape functions for damage detection and localisation in detail.

2.1 Solution of the sensor design problem

In order to find exact solutions of the sensor design problem stated above we apply the principle of virtual work [34] to an auxiliary quasi-static frame structure. The latter is constructed from the original frame structure by using the force method [35] that is frequently used to analyze redundant frame structures, for which the first step is to introduce an auxiliary statically determinate frame structure by releasing kinematical constraints. E.g. clamped conditions are replaced by simply supported ones or intermediate hinges are introduced.

In the principle of virtual work, $\delta W^{(i),aux} + \delta W^{(e),aux} = 0$, we have the virtual work of the internal forces as

$$\delta W^{(i),aux} = \sum_{i=1}^n \left(\int_0^{h_i} M_{iL}^{(qs)} \frac{\partial^2 \delta w_{iL}}{\partial x_{iL}^2} dx_{iL} + \int_0^{h_i} M_{iR}^{(qs)} \frac{\partial^2 \delta w_{iR}}{\partial x_{iR}^2} dx_{iR} \right), \tag{2}$$

in which $M_{i(L,R)}^{(qs)}(x_{i(L,R)})$ is the unique quasi-static bending moment in the statically determinate auxiliary structure due to externally applied auxiliary static forces. $\delta w_{i(L,R)}$ is any kinematically admissible virtual deflection, which in general must satisfy the kinematical boundary conditions and intermediate kinematical constraints of the auxiliary problem. Hence, the deflection of the original problem can be used as the virtual deflection, $\delta w_{i(L,R)} = w_{i(L,R)}(x_{i(L,R)}, t)$. Furthermore, we use the quasi-static bending moments in the auxiliary problem as the sensor shape functions in the original problem, $S_{i(L,R)}(x_{i(L,R)}) = 1 M_{i(L,R)}^{(qs)}(x_{i(L,R)})$; the factor 1 with dimension $[1] = N^{-1}m^{-1}$ ensuring a non-dimensional sensor signal will be omitted in the following. Comparing the resulting form of the virtual work of the internal forces, Eq. (2), with the sensor signal, Eq. (1), we conclude that the sensor signal of a spatial filter measures the work of the external auxiliary static forces applied to the auxiliary quasi-static frame structure on the original deflections; hence, it filters the specific kinematical entity of the original problem, which is the work conjugate of the external forces applied in the auxiliary problem,

$$y(t) = \delta W^{(e),aux} \Big|_{\delta w_{i(L,R)} = w_{i(L,R)}(x_{i(L,R)}, t)} \tag{3}$$

In particular, we use unit auxiliary external forces or moments in the auxiliary problem, which are statically indeterminate entities for the original redundant frame structure. Then their work conjugate deformations (e.g. displacements, jumps in slope) in the original redundant frame structure are trivial (they do vanish), and the sensor signal vanishes as well, $y(t) = 0$; a corresponding sensor design thus is called *nilpotent*. The quasi-static bending moments resulting from the unit auxiliary external forces or moments constitute a basis by means of which any statically indeterminate bending moment in the original frame structure can be represented.

We like to point out that our solution for the sensor design problem has been derived from the principle of virtual work applied to an auxiliary statically determinate problem, but it holds for the original redundant problem under dynamic conditions as well, because we use the original deformations, which are kinematically admissible, as virtual ones in the principle of virtual work. Likewise, the solution does hold as well, when the virtual deformations belong to a structure that follows from the original structure after some selective damage, the reduced structure having a decreased degree of redundancy or being statically determinate. Moreover, the solution can be computed without the need for a full model of the original frame structure, because the auxiliary problem is statically determinate and hence, bending moments can be computed without having to assign any specific material law to the flexible sidewalls. The only model information that is required is purely kinematical; e.g. kinematical boundary conditions as well as intermediate kinematical constraints.

Example problem - a one-storey frame structure As a simple example to illustrate the design method we study a one-storey frame structure made of two flexible sidewalls, which are clamped at their lower side and which are rigidly connected to each other by a rigid floor at their upper side. For the sake of simplicity, the height of the structure and the distance between the sidewalls are $1m$. A sketch of this redundant structure is shown in the left figure of Fig. 2. The right figure of Fig. 2 is the corresponding statically determinate auxiliary problem. The latter is used for computing the quasi-static bending moments, which are then used as sensor shape functions for the original one-storey frame structure. For the sake of computing nilpotent sensor shape functions, either single unit moments at the simply supported lower ends of the sidewalls or a unit bi-moment at the center of the floor are applied in the auxiliary problem. As the corresponding work conjugates are zero in the original frame structure such sensors measure a trivial signal. The resulting bending moments (nilpotent sensor shape functions) are presented in Fig. 3. The corresponding spatial filters, which filter a trivial kinematical entity are also denoted as *Incompatibility Filters*, a notion we will explain in detail in the next section.

3. Structural Health Monitoring using Incompatibility Filters

3.1 Incompatibility filters

In this section we will discuss the notion of a spatial filter put into practice by using nilpotent sensor shape functions as an *Incompatibility Filter*. In order to introduce this notion we start with a simple straight beam of length L , which is clamped at both sides. We apply the principle of virtual work to a quasi-static auxiliary beam. In case the virtual work of the external forces vanishes



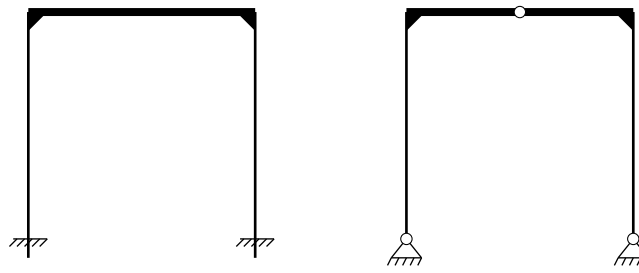


Fig. 2. Original one-storey frame structure (left) and statically determinate auxiliary problem (right)

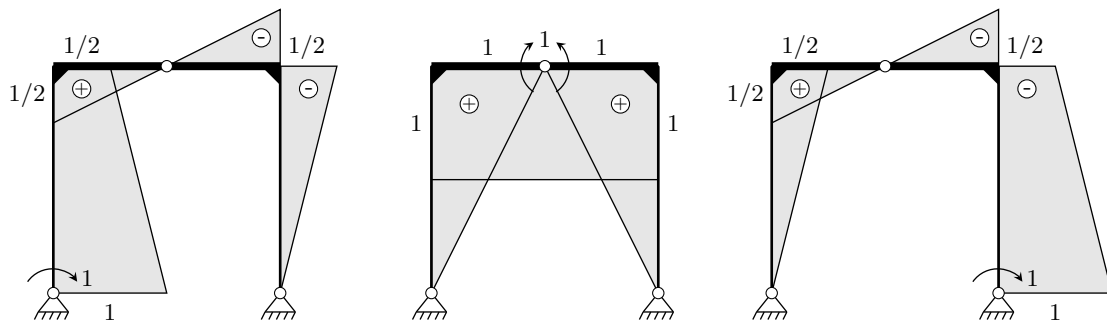


Fig. 3. Nilpotent shape functions for the one-storey frame structure

as no external forces are applied in the auxiliary problem, the virtual work of the internal forces must vanish too,

$$\delta W^{(i),aux} = - \int_0^L M_y^{(sa)}(x) \delta \kappa dx = 0; \quad (4)$$

the beam is assumed inextensible ($EA \rightarrow \infty$) and rigid in shear ($GA \rightarrow \infty$), such that no virtual work from shear forces and normal forces must be accounted for. In contrast to our former derivation for the frame structure, the auxiliary beam is identical to the original one; hence, it is statically indeterminate. Then, $M_y^{(sa)}$ is any statically admissible bending moment, which satisfies $M_y^{(sa)''} = 0$ and $\delta \kappa$ is any kinematically admissible linearized curvature, see [36] for the three-dimensional formulation. $(\%)'$ stands for the partial derivative with respect to the axial coordinate x . Accordingly, the statically admissible bending moment and the kinematically admissible linearized curvature are orthogonal in case no external forces are applied in the auxiliary beam. The notion of a statically admissible bending moment refers to a bending moment, which satisfies the local equilibrium conditions and the dynamical boundary conditions, see [37] for the three-dimensional case. If no external forces are applied this statically admissible bending moment is self-equilibrating. The notion of a kinematically admissible curvature refers to a curvature, which is compatible, and for which the corresponding deflection satisfies the kinematical boundary conditions. One can conclude that, if the virtual curvature $\delta \kappa$ does not satisfy the compatibility conditions, the above orthogonality relation does no longer hold and the virtual work of the internal forces is not trivial any longer, but it is related to the incompatible part of the virtual curvature $\delta \kappa$. This fact also explains our previous notion of an *Incompatibility Filter* for the frame structure; for a more detailed discussion of incompatibility filters in a 3D setting we refer to [14, 38].

We proceed with deriving the local form of the compatibility conditions. Therefore, we integrate the virtual work of the internal forces twice by parts using the actual linearized curvature of the clamped beam as the virtual curvature, $\delta \kappa = -w''$. This results into

$$\delta W^{(i),aux} = \int_0^L M_y^{(sa)} w'' dx = - \left(M_y^{(sa)} w' \right) \Big|_0^L + \left(M_y^{(sa)} w \right) \Big|_0^L - \llbracket M_y^{(sa)} w \rrbracket_{\bar{x}} + \llbracket M_y^{(sa)} w' \rrbracket_{\bar{x}} = 0. \quad (5)$$

Here we have used $M_y^{(sa)''} = 0$. Furthermore, we introduce the statically admissible transverse shear force $Q_z^{(sa)} = M_y^{(sa)'}$ and account for the continuity of both, the statically admissible shear force and bending moment, which finds the orthogonality relation

$$0 = - \left(Q_z^{(sa)} w \right) \Big|_0^L + \left(M_y^{(sa)} w' \right) \Big|_0^L - Q_z^{(sa)}(\bar{x}) \llbracket w \rrbracket_{\bar{x}} + M_y^{(sa)}(\bar{x}) \llbracket w' \rrbracket_{\bar{x}}. \quad (6)$$

We introduce the bending moment at the clamped ends as $M_y^{(sa)}$ in the left clamp and $M_y^{(sa)}$ in the right clamp; then, the second term in the above equation becomes

$$\left(M_y^{(sa)} w' \right) \Big|_0^L = -M_y^{(sa)} w'_0 + M_y^{(sa)} w'_L, \quad (7)$$

and, as the statically admissible transverse shear force is constant we have

$$- \left(Q_z^{(sa)} w \right) \Big|_0^L = Q_z^{(sa)} (w_0 - w_L). \quad (8)$$



Eventually, this results into the final form of the orthogonality relation

$$0 = M_y^{(sa)}(\bar{x})[[w']_{\bar{x}} - M_{y(0)}^{(sa)}w'_0 + M_{y(L)}^{(sa)}w'_L - Q_z^{(sa)}(\bar{x})[[w]_{\bar{x}} + Q_z^{(sa)}w_0 - Q_z^{(sa)}w_L], \tag{9}$$

which holds as long as the kinematically admissible deflection, which in our case is the actual deflection, satisfies the kinematical boundary conditions at the clamped ends, $w_0 = 0, w_L = 0, w'_0 = 0$ and $w'_L = 0$ and the local continuity conditions $[[w']_{\bar{x}} = 0$ and $[[w]_{\bar{x}} = 0$ within the span of the beam.

From this simple example we can easily identify possible damage scenarios, for which spatial filters put into practice by nilpotent sensor shape functions represented by statically admissible bending moments, result into a non-trivial sensor signal; these scenarios are e.g.:

- The homogenous kinematical boundary conditions are not satisfied; e.g. a clamped support is not ideal, but rather replaced by a hinged one with a rotational spring.
- The continuity conditions for the deflection and the slope are not satisfied; e.g. an intermediate hinge is introduced with a rotational spring modeling the residual stiffness.
- The beam is extensible or not rigid in shear.

Each of these scenarios represents a possible damage scenario, or, in the last case, at least a failure in sufficient modeling, under the occurrence of which an *Incompatibility Filter* will render a non-trivial sensor signal. Analogous conditions and damage scenarios can be established for multi-storey frame structures.

3.2 Damage modeling

In the following we will consider only the damage scenario of a hinge with a residual stiffness, because the effect of a crack on the stiffness of a beam can be approximated by a reduction of the stiffness in the vicinity of the crack. A fully local formulation models this stiffness reduction as an intermediate hinge with a rotational spring; the residual spring stiffness K is related to the crack depth d characterized by the non-dimensional ratio $\beta = d/t$ (with the thickness t of the rectangular cross section of the beam) by means of

$$K = \frac{(EJ)}{t} \frac{1}{C(\beta)}. \tag{10}$$

Here, (EJ) is the nominal bending stiffness of the beam cross section. Different methods to compute the non-dimensional local compliance $C(\beta)$ have been reported in the literature; we use the one proposed by [39],

$$C(\beta) = 6\pi\beta^2(0.6384 - 1.035\beta + 3.7201\beta^2 - 5.1773\beta^3 + 7.553\beta^4 - 7.332\beta^5 + 2.4909\beta^6). \tag{11}$$

Although the response of the structure will be affected using other methods to compute the local compliance $C(\beta)$, the methodology for damage detection and localisation, which will be developed in the following, is independent from the specific form of $C(\beta)$.

Example problem We consider the simple one-storey frame structure of height $h = 1\text{m}$, which we have used before. The bending stiffness (EJ) , the linear inertia P and the mass m of the floor are $(EJ) = 1\text{Nm}^2, P = 1\text{kgm}^{-1}$ and $m = 1\text{kg}$. We study only harmonic vibrations, which are excited by a harmonic ground motion of amplitude $W_0 = 0.01\text{m}$ with an excitation frequency ω , which runs from $\omega_s = 1\text{s}^{-1}$ to $\omega_e = 100\text{s}^{-1}$. Three cases are considered - the original undamaged frame structure, a damaged frame structure with one hinge located in the left sidewall at height $x_{L(\text{hinge})} = h/3$ with $\beta = 0.3$, and a damaged frame structure with one hinge located in the left sidewall at height $x_{L(\text{hinge})} = h/3$ with $\beta_L = 0.3$ and a second hinge in the right sidewall at height $x_{R(\text{hinge})} = 2h/3$ with $\beta_R = 0.1$. Now, we use the nilpotent sensor shape functions from Fig. 3 for monitoring the frame structure. As the floor is assumed rigid only contributions to the signals from the flexible sidewalls must be accounted for and no spatial filter must be put into practice for the rigid floor. For the original frame the corresponding signals from the three incompatibility filters are trivial, for the frame with the single hinge in the left sidewall and for the frame with two hinges the three signals are not zero; these signals are shown in Fig. 4 as functions of the excitation frequency ω . Indeed, due to the damage the signals of the incompatibility

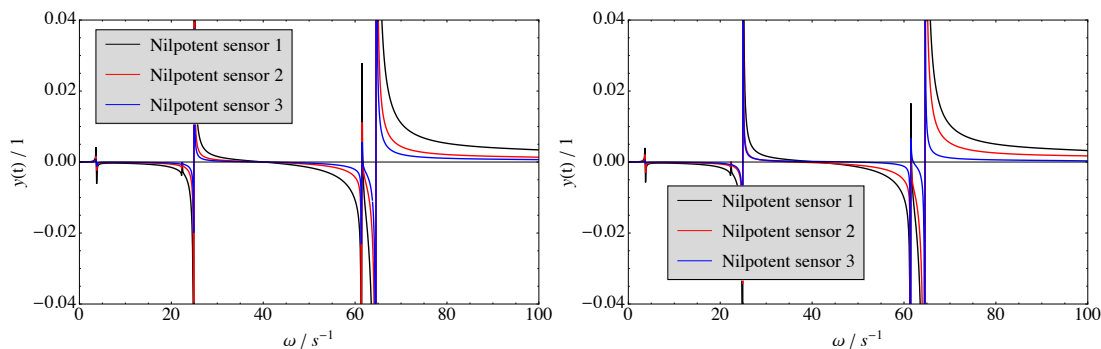


Fig. 4. Signals of the spatial incompatibility filters for the one-storey frame structure: Single hinge (left) and two hinges (right)

filters are not zero and we seek to use the information contained in these signals for structural health monitoring in the following. For that sake, we will introduce a general method for the detection and localisation of local damage put into practice by means of such hinges with residual stiffness for the case of an n -storey frame structure, and show its validity for the damaged one-storey structure, the signals of which are shown in Fig. 4. In order to a-priori quantify the damage in terms of the harmonic response we present the first five natural frequencies in Tab. 1. Note that for the undamaged case, the second and the fourth natural frequency are the first two natural frequencies of a clamped-clamped beam with the bending stiffness and the linear inertia of the flexible sidewalls of the frame structure. We also note that the change in the natural frequencies due to the damage is very small and is therefore not a reliable measure for the detection of damage, as has been pointed out in the literature [40].



	ω_1/s^{-1}	ω_2/s^{-1}	ω_3/s^{-1}	ω_4/s^{-1}	ω_5/s^{-1}
no damage	3.700	22.373	25.000	61.672	64.801
single damage	3.697	22.344	24.957	61.411	64.578
deviation	-0.069%	-0.133%	-0.171%	-0.425%	-0.345%
double damage	3.697	22.340	24.954	61.387	64.543
deviation	-0.080%	-0.147%	-0.182%	-0.463%	-0.399%

Table 1. First five natural frequencies for the one-storey frame structure

3.3 Damage Detection & Localisation

For an n -storey frame structure of the type we are discussing in this paper the grade of redundancy is $3n$; hence, $3n$ nilpotent sensor shape functions can be computed as the $3n$ self-equilibrating statically admissible bending moments of the frame structure. Each of these nilpotent sensor shape functions $S_{nil,i}$ can be used to put 1 incompatibility filter into practice. The corresponding signals are denoted as $y_{nil,i}(t)$, $i = 1, \dots, 3n$. In case of an undamaged frame structure these signals are all trivial. For the damaged frame structure this is not true any more, but some or all of the nilpotent sensor signals render a non-trivial signal. In order to introduce a damage detection and localisation method we define a scalar product for the signals,

$$A_{ij} = \langle y_{nil,i}(t), y_{nil,j}(t) \rangle, \tag{12}$$

the particular form of which will be specified in detail later. In any case this scalar product is zero, if the frame structure is undamaged, because the signals themselves are zero; likewise, any linear combination of these signals

$$\bar{y}_{nil}(t) = \sum_{i=1}^{3n} \alpha_i y_{nil,i}(t) \tag{13}$$

is zero as well. Applying the same linear combination as for the signals to the nilpotent sensor shape functions,

$$\bar{S}_{nil} = \sum_{i=1}^{3n} \alpha_i S_{nil,i} \tag{14}$$

results into a nilpotent sensor shape function. In the damaged frame with intermediate hinges with a rotational spring representing a local damage in terms of a crack some (or all) of the signals from the nilpotent sensors will be non-zero, such that the linear combinations

$$\bar{y}(t) = \sum_{i=1}^{3n} \alpha_i y_{nil,i}(t) \quad \text{and} \quad \bar{S} = \sum_{i=1}^{3n} \alpha_i S_{nil,i} \tag{15}$$

may no longer be a trivial signal nor a nilpotent sensor shape function. However, if the damaged structure with the intermediate hinges is still redundant, there must still exist m nilpotent sensor shape functions, if the remaining degree of redundancy is m . Note that for the damaged structure the notion degree of redundancy refers to the situation, for which the residual spring stiffness is assumed to be zero. E.g., assume that the frame shown in Fig. 2 (right) represents a damaged case of the frame in Fig. 2 (left), then $m = 0$ holds. In the example problems treated in 3.2, but assuming no residual rotational spring stiffnesses to be present, there is $m = 2$ in the first case (one hinge in the left column, single damage case), and $m = 1$ in the second case (one hinge in each of the two columns, double damage). The m nilpotent sensor shape functions for the damaged frame structure must be a linear combination of the original $3n$ nilpotent sensor shape functions and the signals measured from the corresponding m nilpotent sensors must vanish. Therefore, we ask for the linear combination $\bar{y}(t) = \sum_{i=1}^{3n} \alpha_i y_{nil,i}(t)$ to be zero for non-trivial coefficients α_i ; the latter constraint is accounted for as

$$1 = \sum_{i=1}^{3n} \alpha_i^2. \tag{16}$$

We find these coefficients by minimizing the functional

$$J = \langle \bar{y}(t), \bar{y}(t) \rangle - \lambda \left(\sum_{i=1}^{3n} \alpha_i^2 - 1 \right), \tag{17}$$

for which we compute the derivative of the functional with respect to the coefficients of the linear combination and find

$$(\mathbf{A} - \lambda \mathbf{I}) \boldsymbol{\alpha} = \mathbf{0} \tag{18}$$

from $\partial J / \partial \alpha_i = 0$. The components of the $3n \times 3n$ matrix \mathbf{A} are the scalar products A_{ij} defined in Eq. (12) and the components of $\boldsymbol{\alpha}$ are the coefficients α_i . The eigenvalue problem of Eq. (18) has m zero eigenvalues $\lambda_j = 0$, $j = 1, \dots, m$ and the corresponding m eigenvectors $\boldsymbol{\alpha}_j$ contain the coefficients α_i , which can be used in the linear combination of the original nilpotent sensor shape functions to compute the m nilpotent sensor shape functions for the damaged frame structure. From the procedure we just discussed a novel method for the detection and localisation of local damage in frame structures can be derived. Indeed, the information contained in the matrix \mathbf{A} - in particular, the eigenvalues and the eigenvectors - is sufficient for this purpose.



Example problem We compute the matrix \mathbf{A} for our two example problems treated in 3.2. As we are dealing with a problem in the frequency domain, we introduce

$$A_{ij} = \int_{\omega_s}^{\omega_e} y_{nil,i}(\omega)y_{nil,j}(\omega)d\omega, \quad i, j = 1, 2, 3 \tag{19}$$

as a specific inner product of two signals. In the computations the integral is replaced by a sum, for which we compute 200 values in the considered frequency range $\omega = [0.5, \dots, 100]s^{-1}$; hence,

$$A_{ij} = \sum_{k=1}^{200} y_{nil,i}(0.5k)y_{nil,j}(0.5k), \quad i, j = 1, 2, 3, \tag{20}$$

with non-dimensional components A_{ij} of \mathbf{A} . Then, we compute the eigenvalues $\lambda_i, i = 1, 2, 3$, and the corresponding eigenvectors α_i of \mathbf{A} for the two damage scenarios. The results are

$$\mathbf{A} = \begin{bmatrix} 0.207 & 0.083 & 0.041 \\ 0.083 & 0.033 & 0.017 \\ 0.041 & 0.017 & 0.0083 \end{bmatrix},$$

$$\begin{bmatrix} \lambda_1 \\ \lambda_2 \\ \lambda_3 \end{bmatrix} = \begin{bmatrix} 0.248 \\ 0 \\ 0 \end{bmatrix}, \quad \alpha_1 = \begin{bmatrix} -0.913 \\ -0.365 \\ -0.183 \end{bmatrix}, \quad \alpha_2 = \begin{bmatrix} -0.170 \\ -0.068 \\ 0.983 \end{bmatrix}, \quad \alpha_3 = \begin{bmatrix} 0.371 \\ -0.928 \\ 0 \end{bmatrix} \tag{21}$$

for the single damage case, and

$$\mathbf{A} = \begin{bmatrix} 0.217 & 0.114 & 0.026 \\ 0.114 & 0.060 & 0.012 \\ 0.026 & 0.012 & 0.0030 \end{bmatrix},$$

$$\begin{bmatrix} \lambda_1 \\ \lambda_2 \\ \lambda_3 \end{bmatrix} = \begin{bmatrix} 0.279 \\ 0.00109 \\ 0 \end{bmatrix}, \quad \alpha_1 = \begin{bmatrix} -0.882 \\ -0.462 \\ -0.094 \end{bmatrix}, \quad \alpha_2 = \begin{bmatrix} 0.291 \\ -0.690 \\ 0.663 \end{bmatrix}, \quad \alpha_3 = \begin{bmatrix} -0.371 \\ 0.557 \\ 0.743 \end{bmatrix} \tag{22}$$

for the case with two hinges. Note, that the number of non-zero eigenvalues corresponds to the number of local damages, and the eigenvectors with zero eigenvalues are the null space of \mathbf{A} . Also, we mention that units are omitted in the numerical examples.

3.3.1 Damage detection

Damage detection or level 1 structural health monitoring (see [41] for the different levels of structural health monitoring) uses the eigenvalues of the matrix \mathbf{A} to define damage indices D_i ,

$$D_i = \lambda_i, \quad i = 1, \dots, 3n. \tag{23}$$

Zero damage indices for all $i = 1, \dots, 3n$ indicate no damage. In the case of damage on the other hand side, some of the damage indices will be non-trivial, from which we conclude on the presence of damage; in particular, the number of non-zero damage indices corresponds to the number of local damages in terms of intermediate hinges.

Example problem For the specific example problem under consideration the damage indices are presented in Tab. 2. If damage is present, we proceed with the further analysis of the measured signals.

	D_1	D_2	D_3
single damage	0.284	0	0
double damage	0.279	0.00109	0

Table 2. Damage indices for the one-story frame structure

3.3.2 Damage localisation

Damage localisation or level 2 structural health monitoring uses the eigenvectors α_i (with dimension $3n$) of the matrix \mathbf{A} . We arrange these eigenvectors into a matrix \mathbf{T} as

$$\mathbf{T} = \begin{bmatrix} \alpha_1 & \dots & \alpha_{3n-m} & \alpha_{3n-m+1} & \dots & \alpha_{3n} \end{bmatrix} = \begin{bmatrix} \mathbf{T}_{struct} & \mathbf{T}_{nil} \end{bmatrix}. \tag{24}$$

The first $3n - m$ eigenvectors (\mathbf{T}_{struct}) belong to the non-zero eigenvalues and the remaining m eigenvectors (\mathbf{T}_{nil}) to the zero eigenvalues. Introducing the vector of original nilpotent sensor shape functions \mathbf{S}_{nil} as

$$\mathbf{S}_{nil} = \begin{bmatrix} S_{nil,1} & \dots & S_{nil,3n} \end{bmatrix}^T, \tag{25}$$

we compute the nilpotent sensor shape functions for the damaged frame structure from

$$\bar{\mathbf{S}}_{nil} = \mathbf{T}_{nil}^T \mathbf{S}_{nil} = \begin{bmatrix} \bar{S}_{nil,1} & \dots & \bar{S}_{nil,m} \end{bmatrix}^T. \tag{26}$$

As these m nilpotent shape functions correspond to incompatibility filters for the damaged structure, they must be insensitive to the $3n - m$ local hinges, which is possible in general only if there are $3n - m$ common zero values of the m nilpotent shape functions. The zero values of the nilpotent shape functions can then be used to localize the position of the $3n - m$ hinges.



Example problem We show the result for the nilpotent shape functions for the example problem of the one-storey frame structure in Fig. 5. As one can see $m = 2$ nilpotent sensor shape functions exist for the frame structure with one hinge; moreover these two

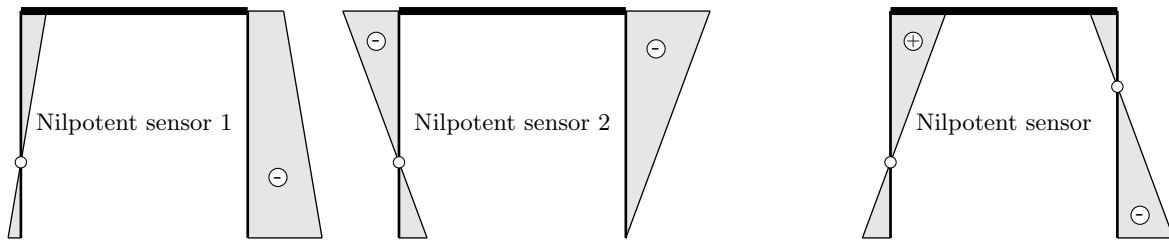


Fig. 5. Nilpotent shape functions for one-storey frame structure with intermediate hinges: Hinge in left sidewall with residual redundancy $m = 2$ and two nilpotent shape functions (left) and hinge in left and right sidewall with residual redundancy $m = 1$ and one nilpotent shape function (right)

shape functions have one common zero value at the location of the hinge in the left sidewall. For the case of two hinges we have only one ($m = 1$) nilpotent sensor shape function with two zero values at the locations of the two hinges. Obviously, the locations of the zero values of the nilpotent sensor shape functions for the damaged frame structure enable the localization of the intermediate hinges; hence, of the local damage.

3.3.3 Monitoring of the damaged frame structure

Besides using the incompatibility filters with the nilpotent shape functions $\bar{\mathbf{S}}_{nil}$ (see also Fig. 5 for the example problem) to further conduct structural health monitoring of the already damaged frame structures, we are also interested to monitor the existing damage in the damaged frames. For that sake we use the transformation with \mathbf{T}_{struct} , which is composed of the eigenvectors of \mathbf{A} with non-zero eigenvalues; hence, we compute $3n - m$ structural shape functions for the damaged frame by means of

$$\mathbf{S}_{struct} = \mathbf{T}_{struct}^T \mathbf{S}_{nil} = \begin{bmatrix} S_{struct,1} & \dots & S_{struct,3n-m} \end{bmatrix}^T. \quad (27)$$

Example problem For the example problem the result is shown in Fig. 6. For the single damage only $3n - m = 1$ such shape functions exist, whereas for the double damage we have $3n - m = 2$ structural shape functions.

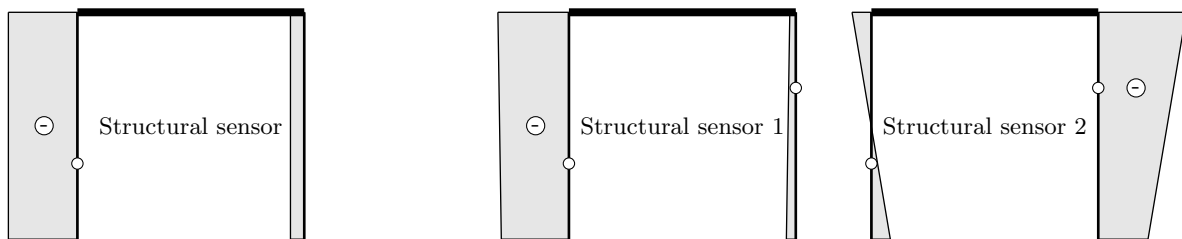


Fig. 6. Structural shape functions for one-storey frame structure with intermediate hinges: Hinge in left sidewall with residual redundancy $m = 2$, $3n - m = 1$ and one structural shape function (left) and hinge in left and right sidewall with residual redundancy $m = 1$, $3n - m = 2$ and two structural shape functions (right)

Putting spatial filters into practice using such structural shape functions results into sensors, for which the signal is proportional to a linear combination of the resulting kinks at the locations of the hinges. This follows from the fact that the intensity of the structural shape functions at the locations of the hinges is not one, and that each of the structural functions has non-zero values at all, or at least at more than one, locations of the hinges. In order to design spatial damage filters, we further apply the transformation

$$\mathbf{S}_{dam} = \mathbf{T}_d \mathbf{S}_{struct} = \begin{bmatrix} S_{dam,1} & \dots & S_{dam,3n-m} \end{bmatrix}^T$$

or equivalently
$$S_{dam,i} = \sum_{j=1}^{3n-m} t_{ij} S_{struct,j}, \quad i = 1, \dots, 3n - m \quad (28)$$

to the structural shape functions resulting into $3n - m$ damage shape functions, which can be used to put spatial damage filters into practice. Here, the $(3n - m) \times (3n - m)$ transformation matrix \mathbf{T}_d is computed from the $3n - m \times 3n - m$ conditions

$$S_{dam,i}(d_i) = 1 \quad \text{and} \quad S_{dam,i}(d_j) = 0, \quad j \neq i \quad \text{and} \quad i, j = 1, \dots, 3n - m, \quad (29)$$

in which d_i represents the position of the i -th damage with $i = 1, \dots, 3n - m$ and $3n - m$ as the number of individual local damages.

Example problem For the example problem, we have $3n - m = 1$ for the single damage and, accordingly the matrix \mathbf{T}_d has only one component, which is

$$t_{11} = -1.095. \quad (30)$$



For the double damage with $3n - m = 2$ the matrix \mathbf{T}_d has four components, which are

$$\begin{aligned} t_{11} &= -1.113, & t_{12} &= -0.054 \\ t_{21} &= 0.137, & t_{22} &= 1.008. \end{aligned} \tag{31}$$

Using the transformation with the computed matrices \mathbf{T}_d for the example problem results into damage shape functions for the spatial damage filters shown in Fig. 7. One can see that in contrast to the shape functions shown in Fig. 6, the shape functions have the intensity one at the location of only one hinge, and the intensity zero at the location of the other hinges.

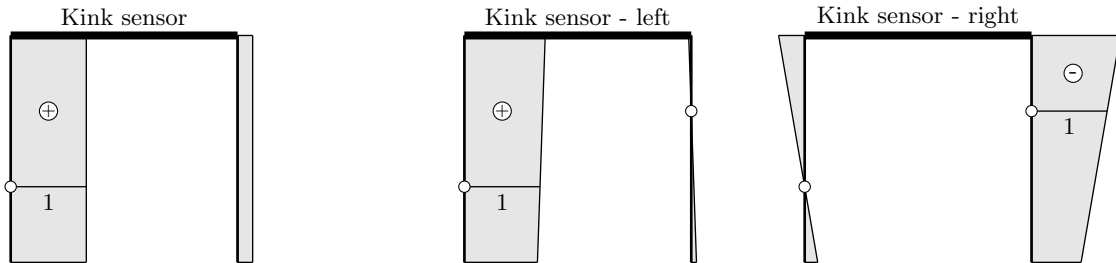


Fig. 7. Damage shape functions for one-storey frame structure with intermediate hinges: Hinge in left sidewall with residual redundancy $m = 2$, $3n - m = 1$ and one damage shape function (left) and hinge in left and right sidewall with residual redundancy $m = 1$, $3n - m = 2$ and two damage shape functions (right)

We further note that the damage shape functions follow from

$$\mathbf{S}_{dam} = \mathbf{T}_d \mathbf{S}_{struct} = \mathbf{T}_d \mathbf{T}_{struct}^T \mathbf{S}_{nil} = \mathbf{T}_{dam}^T \mathbf{S}_{nil} \quad \text{with} \quad \mathbf{T}_{dam} = \mathbf{T}_{struct} \mathbf{T}_d^T, \tag{32}$$

in which we have introduced the transformation matrix $\mathbf{T}_{dam} = \mathbf{T}_{struct} \mathbf{T}_d^T$, by means of which the nilpotent sensor shape functions from the undamaged structure are transformed to the damage shape functions for the damaged frame structure. Finally, we introduce the transformation matrix $\bar{\mathbf{T}}$

$$\bar{\mathbf{T}} = \begin{bmatrix} \mathbf{T}_{dam} & \mathbf{T}_{nil} \end{bmatrix}, \tag{33}$$

by means of which the nilpotent sensor shape functions from the undamaged structure are transformed to both, the damage shape functions and the nilpotent sensor shape functions from the damaged structure. Hence,

$$\mathbf{S}_{new} = \bar{\mathbf{T}}^T \mathbf{S}_{nil} = \begin{bmatrix} \mathbf{S}_{dam}^T & \bar{\mathbf{S}}_{nil}^T \end{bmatrix}^T \tag{34}$$

holds. Moreover, the transformation with $\bar{\mathbf{T}}$ can also be applied to the signals of the original incompatibility filters,

$$\mathbf{y}_{new} = \bar{\mathbf{T}}^T \mathbf{y}_{nil} = \begin{bmatrix} \mathbf{y}_{dam}^T & \bar{\mathbf{y}}_{nil}^T \end{bmatrix}^T. \tag{35}$$

with $\mathbf{y}_{nil} = [y_{nil,1} \dots y_{nil,3n}]^T$ being a column matrix with the signals of the original incompatibility filters as components. The $3n - m$ signals $\mathbf{y}_{dam} = \mathbf{T}_{dam}^T \mathbf{y}_{nil}$ from the damage spatial filters are used to monitor the damage, and the m signals $\bar{\mathbf{y}}_{nil} = \mathbf{T}_{nil}^T \mathbf{y}_{nil}$ from the incompatibility filters for the damaged structure can be used to further detect additional damage. Moreover, we compute a transformed matrix $\bar{\mathbf{A}}$ from the inner product of the transformed signals \mathbf{y}_{new} ,

$$\begin{aligned} \bar{\mathbf{A}} &= \langle \mathbf{y}_{new} \mathbf{y}_{new}^T \rangle = \bar{\mathbf{T}}^T \langle \mathbf{y}_{nil} \mathbf{y}_{nil}^T \rangle \bar{\mathbf{T}} = \bar{\mathbf{T}}^T \mathbf{A} \bar{\mathbf{T}} \\ &= \begin{bmatrix} \mathbf{T}_{dam}^T \\ \mathbf{T}_{nil}^T \end{bmatrix} \mathbf{A} \begin{bmatrix} \mathbf{T}_{dam} & \mathbf{T}_{nil} \end{bmatrix} = \begin{bmatrix} \mathbf{A}_{dam} & \mathbf{0} \\ \mathbf{0} & \mathbf{0} \end{bmatrix} \quad \text{with} \quad \mathbf{A}_{dam} = \mathbf{T}_{dam}^T \mathbf{A} \mathbf{T}_{dam}, \end{aligned} \tag{36}$$

which can alternatively be computed by a transformation of the original matrix \mathbf{A} by means of $\mathbf{A}_{dam} = \mathbf{T}_{dam}^T \mathbf{A} \mathbf{T}_{dam}$, in which \mathbf{A}_{dam} is a $(3n - m) \times (3n - m)$ square matrix. The diagonal elements of $\bar{\mathbf{A}}$ can be used as alternative damage indices \bar{D}_i with $i = 1, \dots, 3n$.

Example problem For the example problem the non-trivial components of the vector of the transformed signals \mathbf{y}_{new} - hence, the components of \mathbf{y}_{dam} - are shown in Fig. 8. For the single damage in the left figure, one damage filter ($3n - m = 1$) measures the kink at the location of the local hinge in the left sidewall, and the two incompatibility filters ($m = 2$) have a trivial signal. For the double damage in the right figure, the two damage filters ($3n - m = 2$) measure the two kinks in the two sidewalls and the one incompatibility filter ($m = 1$) has a trivial signal. Therefore, the resulting spatial damage filters represent sensors, which measure the kinks at the location of the local damage; hence, at the location of the intermediate hinges with residual stiffnesses. The matrices $\bar{\mathbf{A}}$ are

$$\bar{\mathbf{A}} = \begin{bmatrix} 0.298 & 0 & 0 \\ 0 & 0 & 0 \\ 0 & 0 & 0 \end{bmatrix}, \quad \bar{\mathbf{A}} = \begin{bmatrix} 0.346 & -0.0426 & 0 \\ -0.0426 & 0.00633 & 0 \\ 0 & 0 & 0 \end{bmatrix}, \tag{37}$$

and the alternative damage indices \bar{D}_i are presented in Tab. 3 together with the original damage indices D_i . The physical interpretation of the non-zero alternative damage indices \bar{D}_i is strongly related to the measured resulting kinks $y_{new,i} = \llbracket w' \rrbracket_{d_i}$ at the location of the hinges; in particular, we have

$$\bar{D}_i = \langle \llbracket w' \rrbracket_{d_i} \llbracket w' \rrbracket_{d_i} \rangle. \tag{38}$$



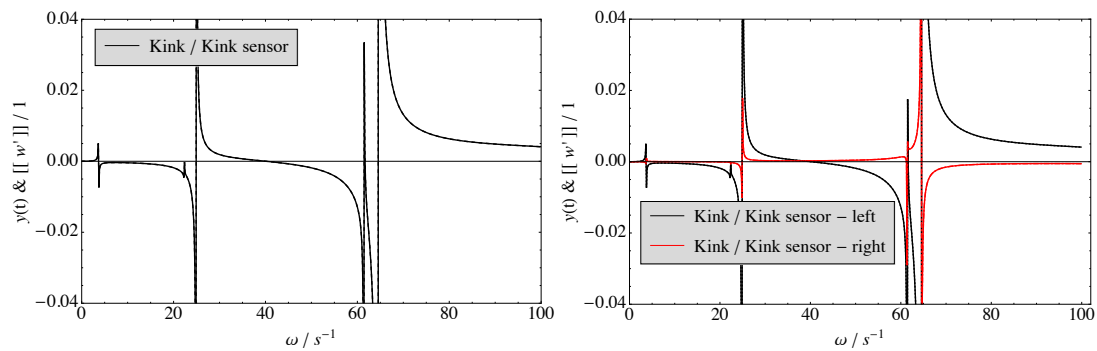


Fig. 8. Signals of the spatial damage filters for the damaged one-storey frame structure: Single hinge (left) and two hinges (right)

	D_1	D_2	D_3	\bar{D}_1	\bar{D}_2	\bar{D}_3
single damage	0.284	0	0	0.298	0	0
double damage	0.279	0.00109	0	0.346	0.00633	0

Table 3. Alternative damage indicis for the simple one-story frame structure

3.3.4 Remark on the example problem

In our example problem concerned with the one-storey frame structure three incompatibility filters were put into practice by means of the three nilpotent shape functions shown in Fig. 3. These shape functions represent statically indeterminate bending moment distributions for the undamaged structure. Hence, any linear combination of the three shape functions results into a nilpotent shape function as well. Keeping in mind the fact that the floor is assumed rigid three such linear combinations are shown in Fig. 9. A design using these three nilpotent sensor shape functions for the incompatibility filters from the very beginning is fully

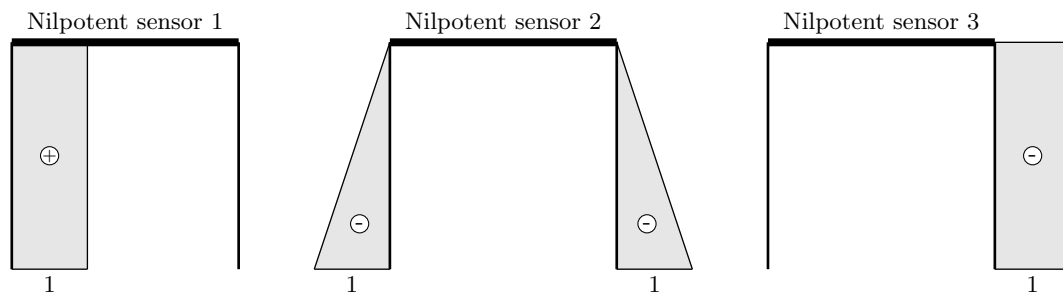


Fig. 9. Alternative nilpotent shape functions for the one-storey frame structure

equivalent to using the original design. Running through the structural health monitoring method introduced above, we will end up with the identical conclusions as before with respect to damage detection, localisation and monitoring. Yet, the design according to Fig. 9 enables a significant simplification of the method. In particular the following points apply.

1. Damage detection: We compute the matrix \mathbf{A} for the two damage scenarios; the result is

$$\mathbf{A} = \begin{bmatrix} 0.298 & -0.199 & 0 \\ -0.199 & 0.133 & 0 \\ 0 & 0 & 0 \end{bmatrix} \quad \text{and} \quad \mathbf{A} = \begin{bmatrix} 0.346 & -0.245 & -0.0426 \\ -0.245 & 0.173 & 0.0305 \\ -0.0426 & 0.0305 & 0.00633 \end{bmatrix}. \quad (39)$$

As nilpotent sensor 1 and nilpotent sensor 3 are already damage / kink sensors for the damaged structure with a hinge in a sidewall the diagonal elements A_{11} and A_{33} of \mathbf{A} are the alternative damage indices $\bar{D}_i = A_{ii}$; hence, due to the design of the nilpotent sensors, it is sufficient to use only two damage indices $\bar{D}_1 = A_{11}$ and $\bar{D}_2 = A_{33}$, which are

$$\bar{D}_1 = 0.298, \quad \bar{D}_2 = 0 \quad \text{and} \quad \bar{D}_1 = 0.346, \quad \bar{D}_2 = 0.00633, \quad (40)$$

see also Tab. 3. We conclude from the damage indices that in the single damage scenario only the left sidewall is damaged ($\bar{D}_2 = 0$), whereas in the double damage scenario both sidewalls are damaged.

2. Damage localization: To localize damage we exclude information from sensors, for which the corresponding diagonal element in the matrix \mathbf{A} is zero. Therefore, we use only

$$\mathbf{A} = \begin{bmatrix} 0.298 & -0.199 \\ -0.199 & 0.133 \end{bmatrix} \quad \text{and} \quad \mathbf{A} = \begin{bmatrix} 0.346 & -0.245 & -0.0426 \\ -0.245 & 0.173 & 0.0305 \\ -0.0426 & 0.0305 & 0.00633 \end{bmatrix} \quad (41)$$



for localisation. In the single damage scenario two nilpotent sensors must still exist for the damaged structure; one of them is the original nilpotent sensor 3, the other one is a linear combination of nilpotent sensor 1 and nilpotent sensor 2

$$\bar{y}_{nil} = \alpha_1 y_{nil,1} + \alpha_2 y_{nil,2}, \tag{42}$$

the signal of which must vanish. To compute non-trivial solutions for α_1 and α_2 , we could solve the eigenvalue problem; yet, we seek a minimum for $\langle \bar{y}_{nil}, \bar{y}_{nil} \rangle$ with the constraint $\alpha_2 = 1$ instead of the original constraint $\alpha_1^2 + \alpha_2^2 = 1$; hence, we minimize the cost function

$$J = \langle \bar{y}_{nil}, \bar{y}_{nil} \rangle + \lambda(\alpha_2 - 1). \tag{43}$$

The result is

$$\alpha = [0.666 \quad 1]^T, \tag{44}$$

from which a new nilpotent sensor is found as $S_{nil,new} = 0.666S_{nil,1} + S_{nil,2}$ replacing the original nilpotent sensor 2. The adjusted sensor design for the single damage scenario is shown in the top of Fig. 10. From the zero of $S_{nil,new}$ (denoted as nilpotent sensor 1 in the figure), which is located at $x_L = 1/3$ we conclude on the location of the hinge. For the double damage scenario we seek a linear combination

$$\bar{y}_{nil} = \alpha_1 y_{nil,1} + \alpha_2 y_{nil,2} + \alpha_3 y_{nil,3} \tag{45}$$

with $\alpha_2 = 1$ by minimizing $\langle \bar{y}_{nil}, \bar{y}_{nil} \rangle$ with the constraint $\alpha_2 = 1$; we find

$$\alpha = [0.666 \quad 1 \quad -0.333]^T, \tag{46}$$

such that $S_{nil,new} = 0.666S_{nil,1} + S_{nil,2} - 0.333S_{nil,3}$ replaces the original nilpotent sensor 2. The adjusted sensor design is shown in the bottom of Fig. 10. The zeros of the new nilpotent sensor shape function at $\bar{x}_L = 1/3$ and $\bar{x}_R = 2/3$ constitute the

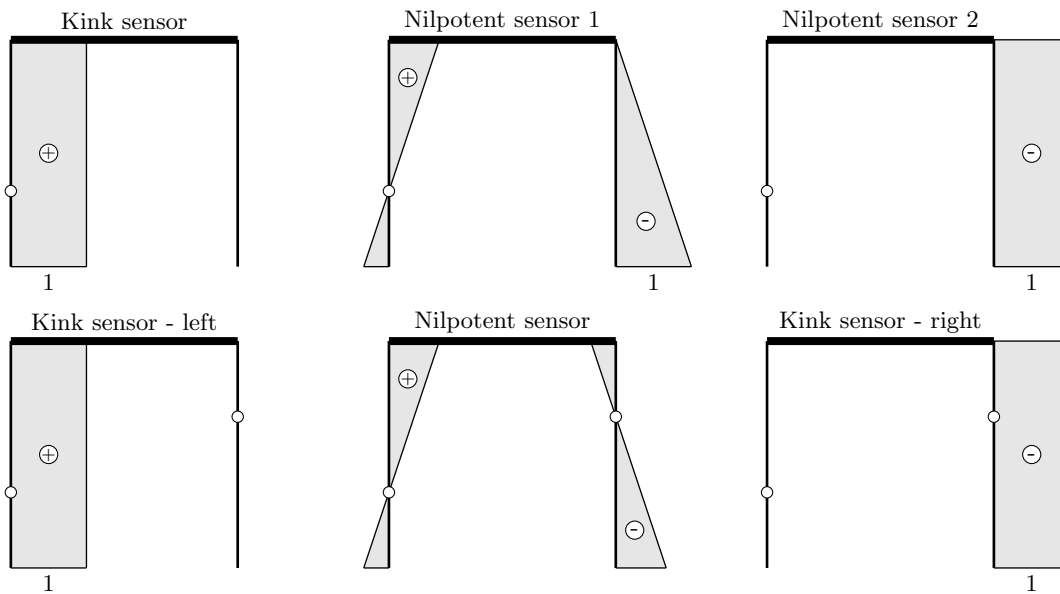


Fig. 10. Alternative damage and nilpotent shape functions for the one-storey frame structure: Single hinge (top) and two hinges (bottom)

position of the two hinges.

3. **Damage monitoring:** The new nilpotent sensor shape functions put incompatibility filters for the damaged frame structures into practice, which are used for structural health monitoring of the already damaged frames. To monitor the damage / kinks no further transformations are needed in this design, as the shape functions with constant intensity in one sidewall only directly result into spatial damage filters monitoring kinks in sidewalls with hinges. Hence, the final adjusted design for the monitoring system for the damaged frame structures is shown in Fig. 10.

Besides the simplification of the method for the one-storey frame structure due to the alternative initial design, this design (Fig. 9) can be used independently for each storey of a multi-storey frame structure. Hence, we will be using this design and the simplified method for structural health monitoring of a three-storey frame structure in the following.

4. Sensor network design

In the previous section we have discussed spatial filters implemented by means of continuously distributed strain-type sensors based on the assumption that we are able to measure the strain (in our case the linearized curvature) in every point of the flexible sidewalls, and furthermore to assign an arbitrary shape function to these measurements resulting into nilpotent sensors used for structural health and damage monitoring.



In this section we consider the problem of putting approximate spatial filters into practice by means of sensor networks. A sensor network is constituted by individual strain-type sensors with constant sensor shape functions located in certain domains of the structure, to which proper constant weights are assigned such that the combined output approximates continuously distributed strain-type sensors. First, each flexible sidewall of the multi-storey frame structure is subdivided into $j = 1, \dots, k$ sub-sections covering the total height of the sidewall. The sub-sections are defined as:

$$\begin{aligned} x_{(L,R)}^{i,j} &\leq x_{i(L,R)} \leq x_{(L,R)}^{i,j} + \Delta x_{(L,R)}^{i,j} = x_{(L,R)}^{i,j+1}, \\ x_{(L,R)}^{i,1} &= 0, \quad x_{(L,R)}^{i,k} + \Delta x_{(L,R)}^{i,k} = x_{(L,R)}^{i,k+1} = h_i. \end{aligned} \tag{47}$$

Next, we assume one strain-type sensor with a constant sensor shape function to be located within each sub-section defined in Eq. (47). Each of these individual sensor patches has the same dimensions covering the total width of the sidewall and its length is $\Delta x \leq \Delta x_{(L,R)}^{i,j}$. Hence, the sections of the patches are: $x_{i,j(L,R)} \leq x_{i(L,R)} \leq x_{i,j(L,R)} + \Delta x$, with $j = 1, \dots, k$. To each patch we assign a constant sensor shape function $S_{i,j(L,R)}$ as a weight such that the sensor signal $\bar{y}(t)$ of the sensor network is

$$\bar{y}(t) = - \sum_{i=1}^n \sum_{j=1}^k \left(S_{i,jL} \int_{x_{i,jL}}^{x_{i,jL} + \Delta x} \frac{\partial^2 w_{iL}}{\partial x_{iL}^2} dx_{iL} + S_{i,jR} \int_{x_{i,jR}}^{x_{i,jR} + \Delta x} \frac{\partial^2 w_{iR}}{\partial x_{iR}^2} dx_{iR} \right). \tag{48}$$

The signal of the original spatial filter with the shape functions $S_{i(L,R)}(x_{i(L,R)})$ can be reformulated as

$$y(t) = - \sum_{i=1}^n \sum_{j=1}^k \left(\int_{x_L^{i,j}}^{x_L^{i,j} + \Delta x_L^{i,j}} S_{iL}(x_{iL}) \frac{\partial^2 w_{iL}}{\partial x_{iL}^2} dx_{iL} + \int_{x_R^{i,j}}^{x_R^{i,j} + \Delta x_R^{i,j}} S_{iR}(x_{iR}) \frac{\partial^2 w_{iR}}{\partial x_{iR}^2} dx_{iR} \right). \tag{49}$$

We define the error signal, which results from approximating the spatial filter by the sensor network as $e(t) = \bar{y}(t) - y(t)$; the latter must be minimized. In the present paper we are not in particular interested in an optimal solution of this minimization problem, but we rather present a simple solution based on statically equivalent force systems introduced in [42], which works quite well in the low frequency regime even for a small number of sensor patches in each sidewall; see also [10] for an application of this method to active noise control of plates. In order to put the solution into practice in the following, we consider the bending stiffness in the sections with sensor patches different from the ones without. Furthermore, the bending moment in each sub-section is assumed to be linear $M_{i,j(L,R)}(x_{i(L,R)}) = a_{i,j(L,R)} + b_{i,j(L,R)}x_{i(L,R)}$, which means that only single forces and moments are applied statically to the frame structure at the interfaces between the sub-sections. Due to the change of the bending stiffness the resulting curvature depends on this bending stiffness

$$\kappa_{i(L,R)} = - \frac{\partial^2 w_{i(L,R)}}{\partial x_{iL}^2} = (EJ)^{-1} M_{i,j(L,R)} = (EJ)^{-1} a_{i,j(L,R)} + (EJ)^{-1} b_{i,j(L,R)} x_{i(L,R)}, \tag{50}$$

where (EJ) is section-wise constant. Inserting the curvature into Eqs. (48) and (49) finds a solution, for which the error $e(t)$ is zero, if the weights $S_{i,j(L,R)}$ and the sensor locations $x_{i,j(L,R)}$ are computed from $2n$ times $2k$ equations, which are

$$\begin{aligned} S_{i,j(L,R)}(EJ)^{-1} \int_{x_{i,j(L,R)}}^{x_{i,j(L,R)} + \Delta x} x_{i(L,R)} dx_{i(L,R)} &= \int_{x_{i,j(L,R)}}^{x_{i,j(L,R)} + \Delta x_{(L,R)}^{i,j}} S_{i(L,R)}(EJ)^{-1} x_{i(L,R)} dx_{i(L,R)}, \\ S_{i,j(L,R)}(EJ)^{-1} \Delta x &= \int_{x_{i,j(L,R)}}^{x_{i,j(L,R)} + \Delta x_{(L,R)}^{i,j}} S_{i(L,R)}(EJ)^{-1} dx_{i(L,R)}. \end{aligned} \tag{51}$$

Again note that (EJ) is included as it is different for different sub-sections. From these equations the locations of the patches $x_{i,j(L,R)}$ and the individual patch weights $S_{i,j(L,R)}$ can be computed. If the patch locations are fixed we use a least square method to solve the $2n$ times $2k$ equations for only $2n$ times k unknowns, which are the individual patch weights $S_{i,j(L,R)}$.

We apply the method to the previously studied example of a one-storey frame structure. For each sidewall three sections of equal length are taken into account and one patch is placed in each of these sections, which has a length of $1/3$ of the section length and which is located in the center of the section. Computing a least square solution for the weights, we can approximate the three sensor shape functions from our previous example shown in Fig. 9; the result is shown in Fig. 11. One can see the effect of the

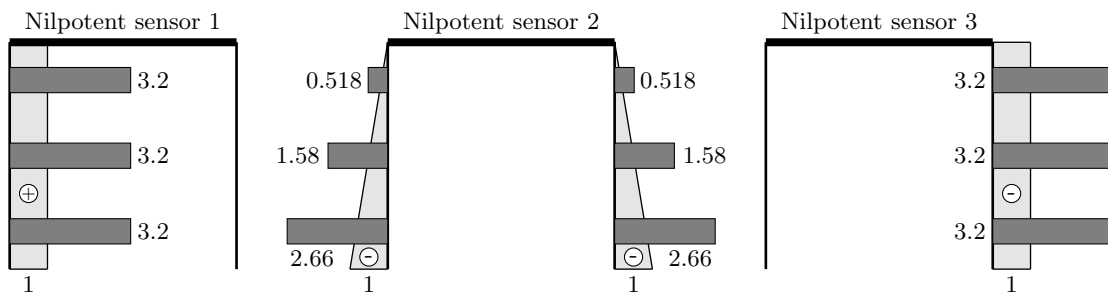


Fig. 11. Approximations of spatial filters by sensor networks for the one-storey frame structure

different bending stiffness in the result for the approximation of the constant shape functions. For a constant bending stiffness one would expect the weights for the approximation of the constant sensor shape functions to be 3; yet, we have the value 3.2 due to the increased stiffness $(EJ) = 1.1(EJ)_0$ in the sections with patches with the bending stiffness $(EJ)_0$ in the sections without patches. In the following we will be using an analogous design for sensor networks for the monitoring of a realistic laboratory three-storey frame structure.



5. Case study: Three-storey frame structure

In order to validate our method for structural health monitoring and damage detection and localisation by piezoelectric sensor networks we consider a three-storey frame structure with three identical storeys and with a harmonic ground excitation. The sidewalls are made of aluminum and three groups of piezoelectric patches (PZT-5A) are mounted to each of the six sidewalls; by group we mean a pair of patches mounted at one position, but on opposite sides of the sidewall in order to remain within the pure bending assumption of the Bernoulli-Euler beam theory. The dimensions of the sidewalls are $0.5m \times 0.04m \times 0.004m$ (height $L \times$ width $d \times$ thickness h) and the ones of the piezoelectric patches are $0.0555m \times 0.04m \times 0.0005m$ (length $\Delta x \times$ width $d_p \times$ thickness h_p). The floor is made of steel with dimensions $0.3m \times 0.04m \times 0.01m$ (length $L_f \times$ width $d_f \times$ thickness h_f); here, the length L_f represents the horizontal distance between the sidewalls. The locations of the three groups of piezoelectric patches $x_{i,1} = L/6 - \Delta x/2$, $x_{i,2} = L/2 - \Delta x/2$ and $x_{i,3} = 5L/6 - \Delta x/2$ are identical for the left and the right sidewall and for each individual storey, $i = 1, 2, 3$. With the material parameters of aluminum and of PZT-5A (see appendix) the bending stiffness $(EJ)_0$ for sections without patches, the corresponding one for sections with patches (EJ) , the mass of the rigid floors M (the floors are assumed rigid in the beam model) and the linear inertia of the sidewalls P_0 and P are given in Tab. 4. Given the bending stiffnesses, we can proceed with the design of the

$(EJ)_0$	(EJ)	M	P_0	P
13.824Nm ²	26.223Nm ²	0.942kg	0.4432kgm ⁻¹	0.7532kgm ⁻¹

Table 4. Parameters for the beam model of the three-storey frame structure

piezoelectric sensor network. We design three nilpotent sensor networks for each storey. The network design follows directly from the previous design of the three nilpotent sensors used for the one-storey frame accounting for different dimensions and bending stiffnesses. The six weights for the three sensor networks (which are identical for each storey) are given in Tab. 5. Numerical results

	$S_{i,1L}$	$S_{i,2L}$	$S_{i,3L}$	$S_{i,1R}$	$S_{i,2R}$	$S_{i,3R}$
nilpotent 1	4.7938	4.7938	4.7938	0	0	0
nilpotent 2	-3.9926	-2.3908	-0.7896	-3.9926	-2.3908	-0.7896
nilpotent 3	0	0	0	-4.7938	-4.7938	-4.7938

Table 5. Weights of the sensor network

are computed using either a transfer matrix formulation within the framework of an electro-mechanically coupled Bernoulli-Euler beam theory [43] or three-dimensional Finite Elements in ANSYS®. For the FE computations 3D 8-node brick elastic elements are used for the sidewalls made of aluminum, 3D 8-node brick piezoelectric elements are used for the 36 piezoelectric patches and the steel floors are also modeled with 3D 8-node brick elastic elements, for which Young's modulus has been assumed sufficiently large to mimic the rigidity of the floors in the beam model. The FE mesh has been chosen to result in a converged solution. In both computations the same sensor weights (see Tab. 5) are used for the sensor networks. A harmonic ground excitation with amplitude $w_0 = 0.001m$ is imposed and - in order to avoid large amplitudes in the vicinity of the natural frequencies - damping is included into the models as one discrete horizontal damper element for each of the three horizontal floor displacements; the damping constant is $d = 10Nsm^{-1}$. As the Finite Element computations render voltages at the piezoelectric patches (open circuit conditions are implemented), we also have to account for a constant factor of proportionality, which depends on the geometry and material parameters, to relate these voltages with the weights given in Tab. 5. For that sake we compute the voltage at an individual patch group ($\bar{x} \leq x \leq \bar{x} + \Delta x$) for the case of an open circuit (for details concerning the sensor equation for piezoelectric patches we refer to Krommer [43]) as

$$V(t) = -\frac{h + h_p}{C} d_p e \int_{\bar{x}}^{\bar{x} + \Delta x} \frac{\partial^2 w}{\partial x^2} dx, \tag{52}$$

in which $C = \eta d_p \Delta \bar{x} h_p^{-1}$ is the capacity of a piezoelectric patch and e and η are a piezoelectric coefficient and a permittivity defined in the appendix. On the other hand, we have the sensor signal from this patch group with the corresponding weight S as

$$y(t) = -S \int_{\bar{x}}^{\bar{x} + \Delta x} \frac{\partial^2 w}{\partial x^2} dx. \tag{53}$$

From a comparison of these two formulations we find a factor κ_V

$$\kappa_V = S \frac{C}{(h + h_p) d_p e}, \tag{54}$$

which we can use as weights for the individual voltages $y^{FE} = \kappa_V V^{FE}$ computed from the three-dimensional Finite Elements and compare the results to the beam solution. In Fig. 12 we show the dynamic magnification factor of the three nilpotent sensor signals for each of the three storeys for the undamaged case. In all results we refer to the transfer matrix formulation as *analytical* and to the three-dimensional Finite Elements as *FEM*. Concerning the results, we note that - due to the symmetry of the problem - nilpotent sensor 2 has a trivial signal and the signals from nilpotent sensor 1 and from nilpotent sensor 3 are identical; hence, there is only one independent signal for each floor. One can observe a very good agreement between the analytical results and the ones computed from the three-dimensional Finite Element computations. Moreover, the signal levels are very small for the nilpotent sensors, if they are compared to signals measured in a damaged frame structure; see the following sections.



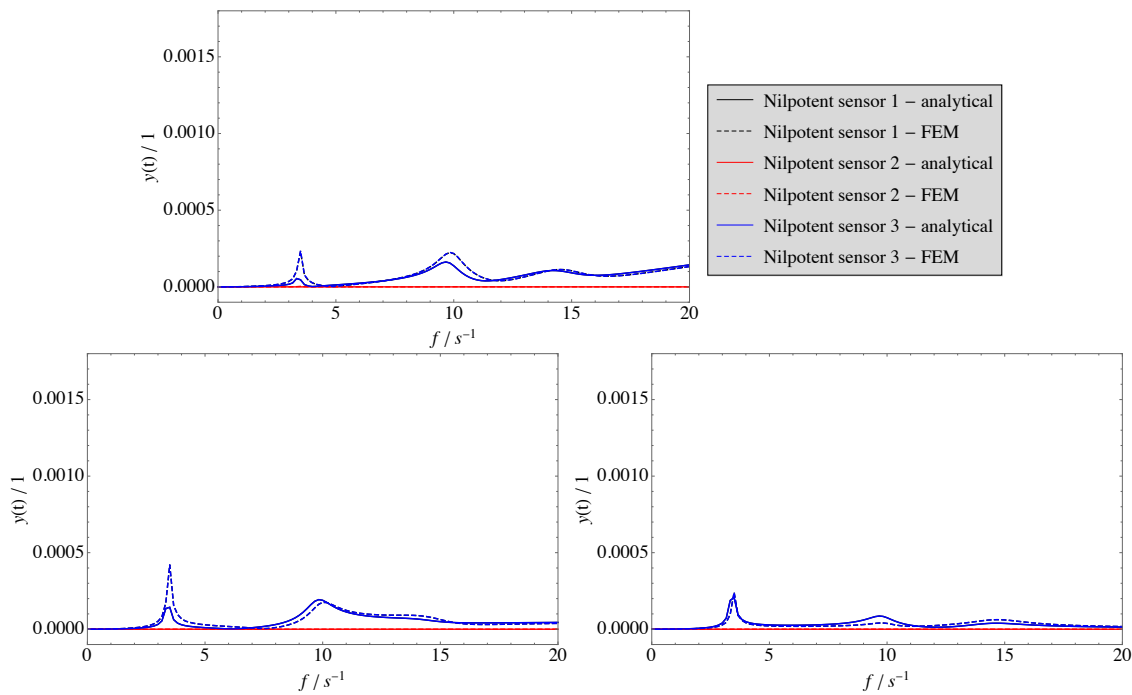


Fig. 12. Nilpotent sensor signals from the incompatibility filters for the three storeys - undamaged frame: First storey (top), second storey (bottom left) and third storey (bottom right)

5.1 Monitoring of a damaged three-storey frame structure

We introduce damage into the frame structure by means of cracks, which are modeled as intermediate hinges with a residual stiffness in the beam model. Hence, we use the damage model of our previous example of the one-storey frame structure. We introduce one intermediate hinge in each storey with a crack depth of $d = 2h/3$. The location of the cracks / hinges are $x_{1,L} = L/6 + \Delta x/2$ in the left sidewall of the first storey, $x_{2,L} = L/6 + \Delta x$ in the left sidewall of the second storey and $x_{3,R} = 5L/6 + \Delta x/2$ in the right sidewall of the third storey. We model the damage in the Finite Element model simply by rigidly connecting only those

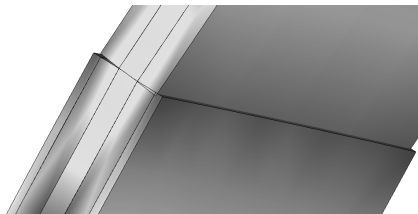


Fig. 13. Detail of a cross section with a crack in the FE model

nodes within the damaged cross section, which have not been reached by the crack, see Fig. 13 for $d = 2h/3$; the rigidly connected part of the cross section is located in the center of the cross section actually modeling two cracks - one on the top and one at the bottom of the cross section. We use the design of the sensor networks from Tab. 5 for each of the three floors and we show the corresponding 9 nilpotent sensor signals from the incompatibility filters in Fig. 14.

One can see that we have a good agreement between the analytical results and the Finite Element ones in most cases. Concerning the results, we note the following:

- The signal level for the nilpotent sensors is much higher than for the original undamaged frame structure. Concerning the first storey this is in particular true for nilpotent sensor 1 and nilpotent sensor 2, because the corresponding sensor shape functions for these two sensors are not trivial in the left sidewall, in which the damage occurs. In contrast, the signal level from nilpotent sensor 3 is still very small and similar to the one for the undamaged frame. From the results for the first storey, we can conclude on the presence of damage in the left sidewall of the first storey and, hence, detect the damage. Concerning the third storey similar arguments lead to the conclusion that the damage must be in the right sidewall. The results for the second storey are not so clear, but still allow to conclude on damage in the left sidewall, because of a comparably small signal level for nilpotent sensor 3.

Finally, we show the signal from nilpotent sensor 1 for the first storey again in Fig. 15 together with the actual kink at the location of the intermediate hinge computed with the transfer matrix formulation. We can see that the signals and the kink are very close. Hence, the originally nilpotent sensor becomes a kink sensor for the damaged structure, which additionally adds to the superiority of nilpotent sensors for structural health monitoring over e.g. displacement sensors, as the signal from the damaged frame has a clear mechanical interpretation. Rather than to further discuss the signals, we now proceed to using the method we have developed in this paper.



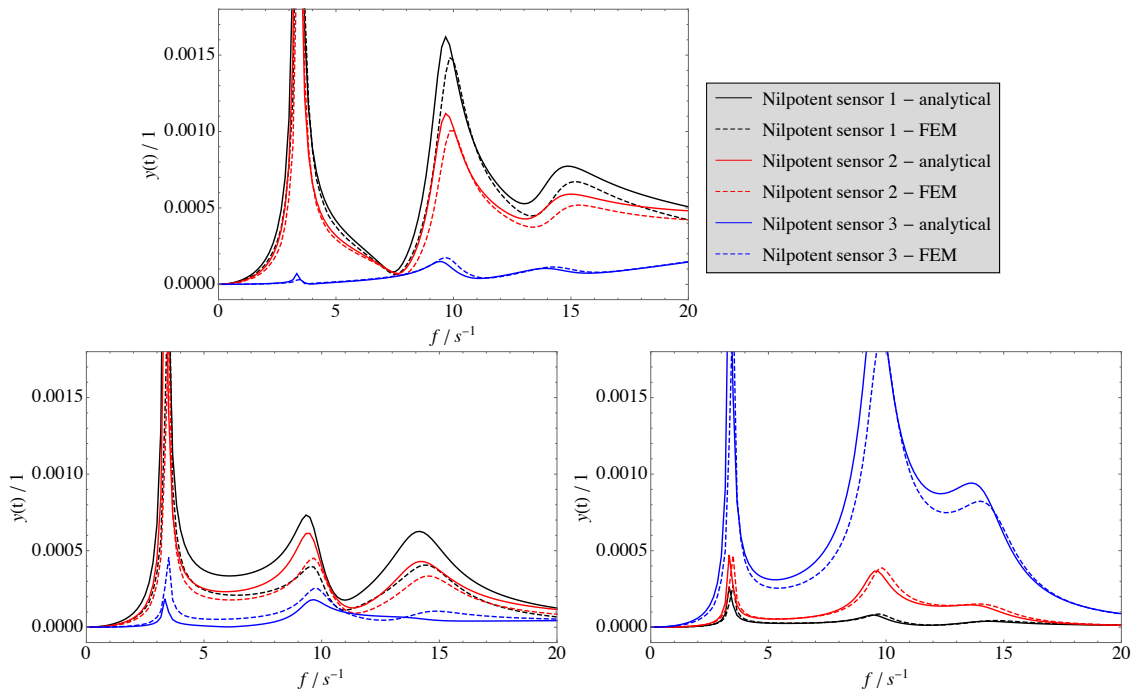


Fig. 14. Nilpotent sensor signals from the incompatibility filters for the three storeys - damaged frame: First storey (top), second storey (bottom left) and third storey (bottom right)

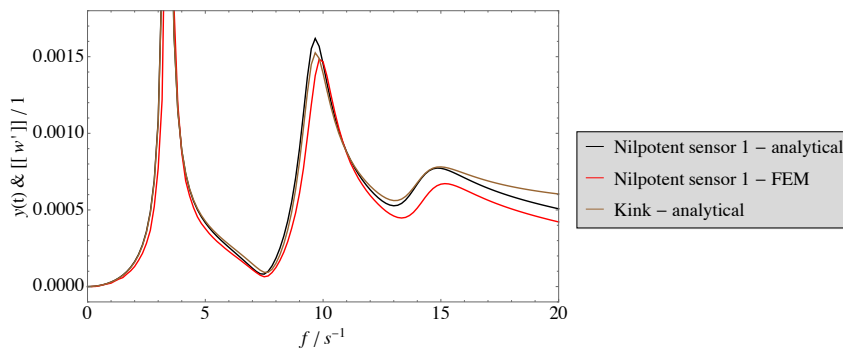


Fig. 15. Signals from nilpotent sensor 1 and kink in the left sidewall of the first storey - damaged frame

Damage detection We use the diagonal elements A_{ii}^j of the matrix A^j as damage indices for each floor with $j = 1, 2, 3$; yet, in this example, we introduce a relative damage index as

$$\bar{D}_i^j = \frac{A_{ii, \text{damaged}}^j}{A_{ii, \text{undamaged}}^j}, \tag{55}$$

because the damage indices are not zero in the undamaged structure. Due to the symmetry in the present problem of a three-storey frame structure, the indices \bar{D}_2^j are infinitely large, because $A_{22, \text{undamaged}}^j$ is zero; hence, we only use two damage indices for each floor. The results for the six damage indices are presented in Tab. 6 using either the data from the beam model or from the Finite Element one; the computation of the components of the matrices A^j uses a total of 120 measurement points in the frequency range $f = [0, \dots, 20]$ Hz.

Damage indices	$\bar{D}_{1(L)}$	$\bar{D}_{1(R)}$	$\bar{D}_{2(L)}$	$\bar{D}_{2(R)}$	$\bar{D}_{3(L)}$	$\bar{D}_{3(R)}$
analytical	88.3	0.97	42.8	0.92	0.97	231.4
Finite Elements	83.3	0.86	20.4	1.68	1.31	313.5

Table 6. Damage indices for three-story frame structure

Damage localisation and monitoring As we have discussed in detail our method is also capable to proceed from a level 1 SHM system for damage detection to a level 2 system, which also allows the localisation of damage. This step was based on the computation



Location	$x_{1(L)}/m$		$x_{2(L)}/m$		$x_{3(R)}/m$	
Error		$e_{1(L)}$		$e_{2(L)}$		$e_{3(R)}$
actual	0.111	-	0.139	-	0.444	-
identified analytical	0.129	3.6%	0.153	2.8%	0.424	-4.0%
identified Finite Elements	0.126	3.0%	0.177	7.6%	0.401	-8.6%

Table 7. Actual and identified damage location with relative errors

of the matrix \mathbf{A} . For the three-storey frame structure the specific design of nilpotent sensors results into three matrices \mathbf{A}^j with the dimension 3×3 and $j = 1, 2, 3$; one for each floor of the structure.

For localisation we are using the simplified method discussed above. In any of the three storeys one sidewall is undamaged as indicated by the those damage indices in Tab. 6, which are close to 1. The corresponding signals are excluded in the computation of \mathbf{A}^j , such that we have matrices with only 2×2 components for each storey. Following the simplified method finds vectors α^j with the coefficients of the proper linear combinations of the sensor signals to produce minimized signals. The identical linear combinations applied to the underlying sensor shape functions finds new nilpotent sensor shape functions, the zeros of which are the location of the damage / hinge. In Tab. 7 the identified damage locations are presented in comparison to the actual ones. One can see that the location of the three local damages / hinges are accurately identified by both the beam model and the FEM model. The error we present is defined as $e_i = (x_{i,\text{identified}} - x_{i,\text{actual}})/L$.

Damage monitoring is done using the original design for the two sensors with a constant sensor shape function in one sidewall and with a new adjusted sensor network that follows from using the components of α^j also as coefficients for a linear combination of the original networks. For the first storey we show the signals of the adjusted monitoring system that are computed for the damaged frame in Fig. 16. Clearly, nilpotent sensor 1 becomes a kink sensor, nilpotent sensor 3 remains a nilpotent sensor and the adjusted nilpotent sensor 2 is a new nilpotent sensor to monitor the residual structural health of the damaged structure. Similar results are obtained for the other two storeys. It is worth noting that these results clearly show the ability of the proposed methodology

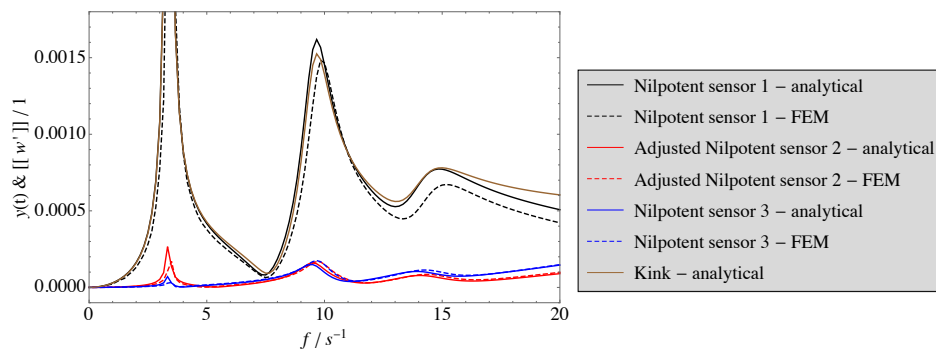


Fig. 16. Signals from adjusted sensor network for the first storey - damaged frame

not only to detect and locate damage, but also to adjust the monitoring system for a damaged structure, for which - besides further health monitoring - one can even monitor the already existing damage. Although the monitoring system itself is designed within the framework of Bernoulli-Euler beam theory, it can be used for the more complex three-dimensional Finite Element model, in which no assumptions on the specific kinematic approximation nor on the local compliance, see eq. (11), to approximate the residual stiffness in a cracked cross section are imposed.

Parameter variation As we already mentioned the non-dimensional crack depth-to-thickness ratio is $\beta = 2/3$ in this example and damage is introduced in the left sidewall of the first and the second storey as well as in the right sidewall of the third storey. This damage scenario is easily detected from the numerical values of the damage indices in Tab. 6. To further study the suitability of the damage index to detect damage, the influence of the variation of β on the sensitivity of the damage index is studied next using the beam model. Therefore, β is varied by steps of 0.1 within the range of $[0.1, \dots, 0.9]$. Fig. 17 shows the damage indices for a single damage in the left sidewall of the first storey for different values of β ; no damage is present in the other two storeys. An exponential sensitivity of the damage index can be seen; nonetheless, a certain damage level is needed to detect the damage. In this example the damage level should at least be $\beta = 0.2$. Next, we also use damage in the other two storeys; in particular in the left sidewall of the second storey and the right sidewall of the third storey. The damage level is simultaneously varied for all three damaged sidewalls. The results for the damage indices are shown in Fig. 18. One can see that the additional damage has no effect on the damage indices of the first storey, but only on the corresponding ones in the second and third storeys; again an exponential sensitivity is observed and a certain minimum damage level is needed for damage detection.

Besides changing the level of damage, we also study the effect of damage position. In the first and second storey the damage location remains fixed, but the location of the simulated damage in the third storey is varied from a location at the lower end of the sidewall to a location at the upper end of the sidewall; the damage level is $\beta = 2/3$ for all three damages. The identified locations using the transfer matrix formulation are shown in Fig. 19 together with the simulated locations at $x = iL/9$ with $i = [0, 1, \dots, 9]$, which are the corresponding points at the dashed line. The error of the identified damage location has a minimum in the middle of the sidewall, and a maximum at the two ends of the sidewalls. In contrast, the corresponding damage indices are largest for the damage located at the two ends and smallest for the middle of the sidewall, see Fig. 20. However, for any damage location the damage index is sufficiently large to detect and locate the damage.



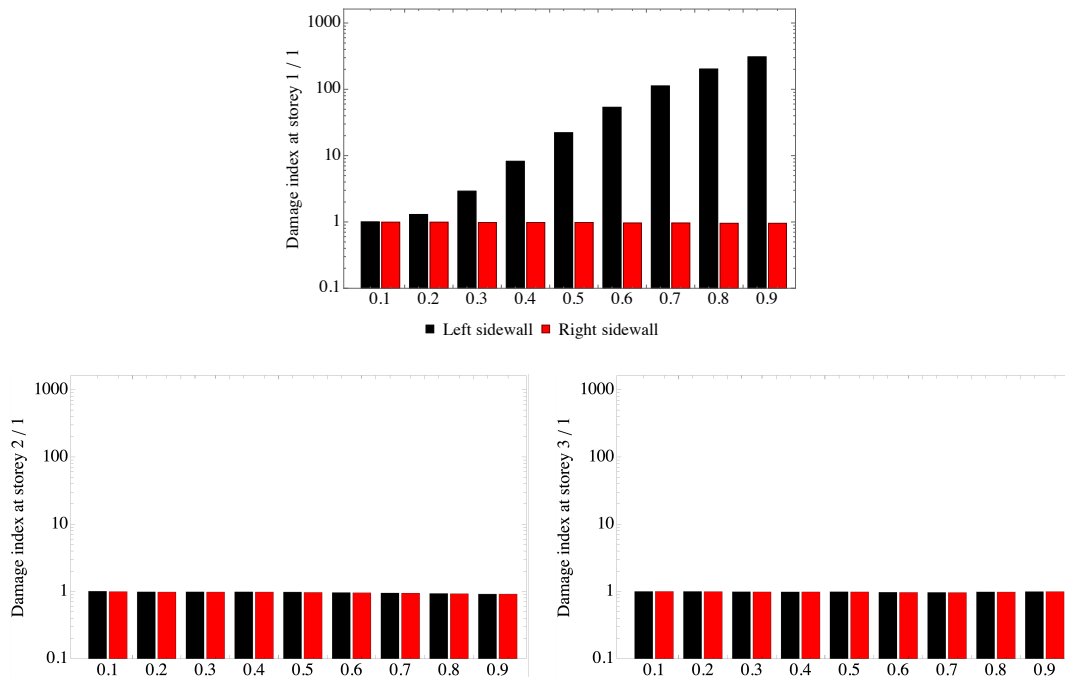


Fig. 17. Damage indices during variation of $\beta = [0.1, \dots, 0.9]$ for damage in the first storey only: First storey (top), second storey (bottom left) and third storey (bottom right)

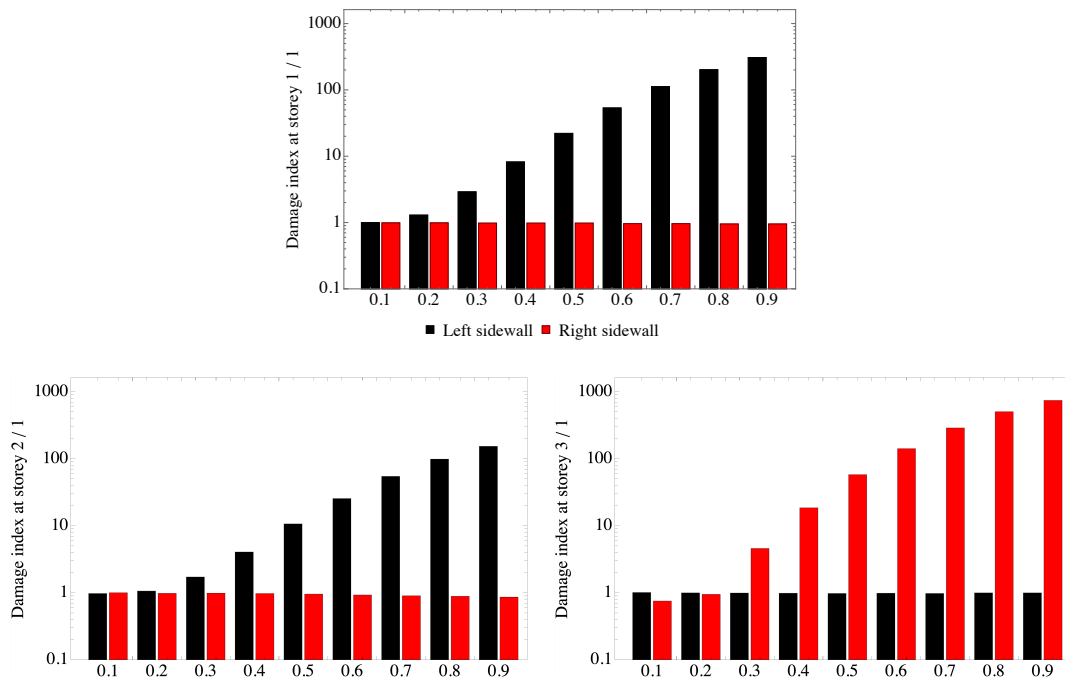


Fig. 18. Damage indices during simultaneous variation of $\beta = [0.1, \dots, 0.9]$ for damage in each storey: First storey (top), second storey (bottom left) and third storey (bottom right)

6. Conclusions

In the present paper we have developed a novel method for structural health monitoring of multi-storey frame structures using so-called incompatibility filters. It has been shown that the method is able to detect and locate local damage in multi-storey frame structures with sufficient accuracy. Moreover, the design of incompatibility filters put into practice by piezoelectric sensor networks, which was based on the Bernoulli-Euler beam theory, was also tested on a three-dimensional Finite Element model for a three-storey frame structure; here, we were able to numerically proof the concept of incompatibility filters for structural health monitoring. Although this proof of concept only considered the case of a harmonic ground excitation, the developed methodology is actually independent from the specific type of excitation, and it works for both, static and dynamic excitations.

Moreover, the developed methodology does not require a full mechanical model of the actual structure in the sense that constitutive relations are needed, but only a kinematic model in the sense that such a model enables us to introduce the notion of a self-equilibrating bending moment. A forthcoming extension towards the more realistic case of three-dimensional frame structures with possibly flexible floors is expected to be straightforward as long as the concept of self-equilibrating forces and moments



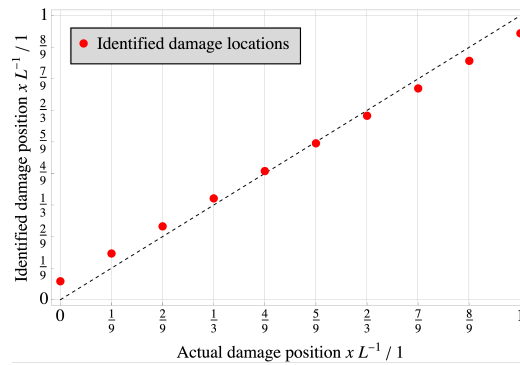


Fig. 19. Localisation of varying damage position in the third floor

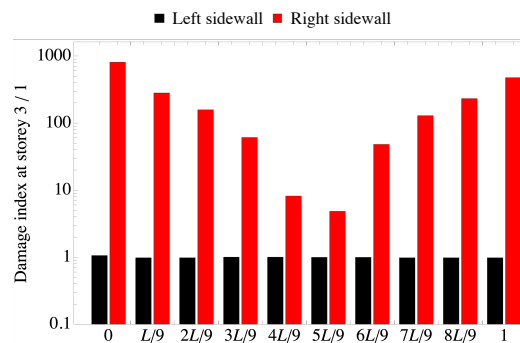


Fig. 20. Damage index during variation of the damage position in the third floor

is applicable. We are positive that the method itself is even applicable to real engineering systems as self-equilibrating forces and moments / stresses exist also in such systems, which is imperative to put incompatibility filters into practice. Also, we wish to point out that within this paper we have developed the methodology without any further processing of the signals from the incompatibility filters, which is left for future research with respect to our method working under realistic operating conditions as well. Besides these aspects, which encourage us to proceed our research, a main issue that must be addressed in the future is the need for a spatial filtering system put into practice either continuously distributed or as a dense sensor network.

Author Contributions

M. Krommer was responsible for the theoretical part of the paper and computed the results for the example problem concerned with the one-storey frame structure; M. Zellhofer conducted the Finite Element computations and was responsible for the three-storey frame structure case study; H. Irschik supported the theoretical developments and provided the fundamental ideas, on which the paper is based on. The manuscript was written through the contribution of all authors. All authors discussed the results, reviewed and approved the final version of the manuscript.

Conflict of Interest

The authors declared no potential conflicts of interest with respect to the research, authorship and publication of this article.

Funding

The authors acknowledge the support by the Linz Center of Mechatronics (LCM) in the framework of the Austrian COMET-K2 program.

References

- [1] Crawley, E.F., Intelligent Structures for Aerospace: A Technology Overview and Assessment, *AIAA Journal*, 32(8), 1994, 1689–1699.
- [2] Tani, J., Takagi, T., Qiu, J., Intelligent material systems: application of functional materials, *Applied Mechanics Review*, 51, 1998, 505–521.
- [3] Liu, S.-C., Tomizuka, M., Ulsoy, G., Strategic Issues in Sensors and Smart Structures, *Proceedings of the 3rd European Conference on Structural Control*, July 2004, Vienna, Austria, 4 pages, 2004.
- [4] Liu, S.-C., Tomizuka, M., Ulsoy, G., Challenges and Opportunities in the Engineering of Intelligent Structures, *Smart Structures and Systems*, 1(1), 2005, 1–12.
- [5] Gabbert, U., Tzou, H.S., Preface, *Proceedings of the IUTAM-Symposium on Smart Structures and Structronic Systems*, September 2000, Magdeburg, Germany, 2001.
- [6] Glaser, S.D., Shoureshi, R.A., Pescovitz, D., Frontiers in Sensors and Sensing Systems, *Smart Structures and Systems*, 1(1), 2005, 103–120.
- [7] Gopinathan, S.V., Varadan, V.V., Varadan, V.K., Active Noise Control Studies Using the Rayleigh-Ritz Method, *Proceedings of the IUTAM-Symposium on Smart Structures and Structronic Systems*, September 2000, Magdeburg, Germany, 2001.
- [8] Irschik, H., Krommer, M., Nader, M., Pichler, U., Dynamic piezoelectric shape control applied of shells of revolution with translatory support excitation, *Proceedings of the US - Europe Workshop on Sensors and Smart Structures Technology*, April 2002, Como, Italy, 2003.
- [9] Alkhatib, R., Golnaraghi, M.F., Active Structural Vibration Control: A Review, *The Shock and Vibration Digest*, 35(5), 2003, 367–383.



- [10] Zenz, G., Berger, W., Gerstmayr, J., Nader, M., Krommer, M., Design of piezoelectric transducer arrays for passive and active modal control of thin plates, *Smart Structures and Systems*, 12(5), 2013, 547–577.
- [11] Lee, C.-K., Moon, F.C., Modal Sensors/Actuators, *Journal of Applied Mechanics*, 57(2), 1990, 434–441.
- [12] Krommer, M., Irschik, H., Sensor and Actuator Design for Displacement Control of Continuous Systems” *Smart Structures and Systems*, 3(2), 2007, 147–172.
- [13] Preumont, A., Francois, A., De Man, P., Loix, N., Henriouille, K., Distributed sensors with piezoelectric films in design of spatial filters for structural control, *Journal of Sound and Vibration*, 282, 2005, 701–712.
- [14] Krommer, M., Vetyukov, Yu., A novel damage detection method based on spatial compatibility filtering, *Proceedings of 13th Mechatronics Forum International Conference (Mechatronics 2012)*, September 2012, Linz, Austria, 8 pages, 2012.
- [15] Irschik, H., Krommer, M., Belyaev, A.K., Schlacher, K., Shaping of Piezoelectric Sensors/Actuators for Vibrations of Slender Beams: Coupled Theory and Inappropriate Shape Functions, *Journal of Intelligent Materials Systems and Structures*, 9, 1998, 546–554.
- [16] Preumont, A., Francois, A., De Man, P., Piefort, V., Spatial filters in structural control, *Journal of Sound and Vibration*, 265, 2003, 61–79.
- [17] Deraemaeker, A., Preumont, A., Vibration based damage detection using large array sensors and spatial filters, *Mechanical Systems and Signal Processing*, 20, 2006, 1615–1630.
- [18] Tondreau, G., Deraemaeker, A., Spatial Filtering for Structural Health Monitoring, *Encyclopedia of Earthquake Engineering*, Springer, Berlin, Heidelberg, 2014.
- [19] Deraemaeker, A., Worden, K., *New Trends in Vibration Based Structural Health Monitoring*, Springer, Vienna, 2010.
- [20] Mendrok, K., Uhl, T., Maj, W., Packo, P., SHM system based on modal filtration, *Key Engineering Materials*, 518, 2012, 289–297.
- [21] Mendrok, K., The Application of Spatial Filtration for Damage Detection in Structures with Multiple Poles, *Proceedings of the 13th International Conference on Damage Assessment of Structures: DAMAS 2019, 9-10 July 2019, Porto, Portugal*, Lecture Notes in Mechanical Engineering, Springer Nature, Singapore, 2020.
- [22] Irschik, H., Krommer, M., Vetyukov, Yu., On the Use of Piezoelectric Sensors in Structural Mechanics: Some Novel Strategies, *Sensors*, 10, 2010, 5626–5641.
- [23] Preumont, A., De Man, P., Francois, A., Loix, N., Henriouille, K., Spatial Filtering with Discrete Array Sensors and Distributed PVDF Films, *Advances in Smart Technologies in Structural Engineering*, Computational Methods in Applied Sciences, 1, Springer, Berlin, Heidelberg, 2004.
- [24] Qing, X., Li, W., Wang, Y., Sun, H., Piezoelectric Transducer-Based Structural Health Monitoring for Aircraft Applications, *Sensors*, 19, 545, 2019, 27 pages.
- [25] B.F. Spencer, jr., M.E. Ruiz-Sandoval and N. Kurata, "Smart Sensing Technology: Opportunities and challenges", *Structural Control and Health Monitoring* 11, pp. 349-368, 2004.
- [26] Gupta, V., Sharma, M., Thakur, N., Optimization criteria for optimal placement of piezoelectric sensors and actuators on a smart structure: a technical review, *Journal of Intelligent Material Systems and Structures*, 21, 2010, 1227–1243.
- [27] Porn, S., Nasser, H., Coelho, R.F., Belouettar, S., Deraemaeker, A., Level set based structural optimization of distributed piezoelectric modal sensors for plate structures, *International Journal of Solids and Structures*, 80, 2016, 348–358.
- [28] Wildy, S., Koutousov, A., Codrington, J., A new passive defect detection technique based on the principle of strain compatibility, *Smart Materials and Structures*, 17(4), 2008, 045004.
- [29] Wildy, S., Codrington, J., An Algorithm for Identifying a Crack Within a Measured Displacement Field, *Journal of Nondestructive Evaluation*, 36, 37, 2017, 10 pages.
- [30] Krommer, M., Zellhofer, M., Design of piezoelectric sensor networks for structural monitoring of frame structures, CD-Rom Proceedings of COMP-DYN 2009 - ECCOMAS Thematic Conference on Computational Methods in Structural Dynamics and Earthquake Engineering, June / July 2009, Rhodes, Greece, 8 pages, 2012.
- [31] Krommer, M., Zellhofer, M., Piezoelectric sensor networks for structural and health monitoring of multi-storey frame structures: Numerical and experimental verification, *Proceedings of the 5th European Workshop on Structural Health Monitoring*, June / July 2010, Sorrento, Italy, 634–640, 2010.
- [32] Krommer, M., Zellhofer, M., Numerical and experimental verification of piezoelectric sensor networks for health monitoring and control of frame structures, *Proceedings of the 4th International Conference on Experimental Vibration Analysis for Civil Engineering Structures (EVACES 2011)*, October 2011, Varenna, Italy, 585–592, 2011.
- [33] Caddemi, S., Calio, I., Exact solution of the multi-cracked Euler-Bernoulli column, *International Journal of Solids and Structures*, 45, 2008, 1332–1351.
- [34] Ziegler, F., *Introduction to the Mechanics of a Continuous Medium*, Springer, New York, 1995.
- [35] Krenk, S., Høgsberg, J., *Statics and Mechanics of Structures*, Springer, Dordrecht, 2013.
- [36] Malvern, L.E., *Mechanics of Solids and Fluids*, Prentice-Hall, Englewood Cliffs, N.J., 1969.
- [37] Gurtin, M.E., *The Linear Theory of Elasticity, Linear Theories of Elasticity and Thermoelasticity*, Springer, Berlin, Heidelberg, 1973.
- [38] Krommer, M., Irschik, H., Design of Piezoelectric Sensors for Structural and Health Monitoring based on the Principle of Virtual Work, *Advanced Materials Research*, 745, 2013, 73–87.
- [39] Ostachowicz, W.M., Krawczuk, C., Analysis of the effect of cracks on the natural frequencies of a cantilever beam, *Journal of Sound and Vibration*, 150(2), 1991, 191–201.
- [40] Deraemaeker, A., Reynders, E., De Roeck, G., Kullaa, J., Vibration-based structural health monitoring using output-only measurements under changing environment, *Mechanical Systems and Signal Processing*, 22(1), 2008, 34–56.
- [41] Farrar, C.R., Worden, K., An introduction to structural health monitoring, *Philosophical Transactions of the Royal Society A*, 365, 2006, 303–315.
- [42] Krommer, M., Zellhofer, M., Heilbrunner, K.-H., Strain-type sensor networks for structural monitoring of beam-type structures, *Journal of Intelligent Material Systems & Structures*, 20, 2009, 1875–1888.
- [43] Krommer, M., On the correction of the Bernoulli-Euler beam theory for smart piezoelectric beams, *Smart Materials and Structures*, 10(4), 2001, 668–680.

ORCID iD

Michael Krommer  <https://orcid.org/0000-0003-2753-1090>

Markus Zellhofer  <https://orcid.org/0000-0002-5487-9271>

Hans Irschik  <https://orcid.org/0000-0001-6593-243X>



© 2021 by the authors. Licensee SCU, Ahvaz, Iran. This article is an open access article distributed under the terms and conditions of the Creative Commons Attribution-NonCommercial 4.0 International (CC BY-NC 4.0 license) (<http://creativecommons.org/licenses/by-nc/4.0/>)

How to cite this article: Michael Krommer, Markus Zellhofer, Hans Irschik. Structural Health Monitoring of Multi-Storey Frame Structures using Piezoelectric Incompatibility Filters: Theory and Numerical Verification, *J. Appl. Comput. Mech.*, 7(SI), 2021, 1138–1157. <https://doi.org/10.22055/JACM.2020.33246.2186>



Appendix A

For a transversally isotropic piezoelectric material with the remanent polarization in the 3-direction (such as PZT-5A) the linearized three dimensional constitutive relations can be written in matrix form as

$$\begin{bmatrix} \sigma_{11} \\ \sigma_{22} \\ \sigma_{33} \\ \sigma_{23} \\ \sigma_{13} \\ \sigma_{12} \\ D_1 \\ D_2 \\ D_3 \end{bmatrix} = \begin{bmatrix} Q_{11} & Q_{12} & Q_{13} & 0 & 0 & 0 & 0 & 0 & -e_{31} \\ Q_{12} & Q_{11} & Q_{13} & 0 & 0 & 0 & 0 & 0 & -e_{31} \\ Q_{13} & Q_{13} & Q_{33} & 0 & 0 & 0 & 0 & 0 & -e_{33} \\ 0 & 0 & 0 & Q_{44} & 0 & 0 & 0 & -e_{15} & 0 \\ 0 & 0 & 0 & 0 & Q_{44} & 0 & -e_{15} & 0 & 0 \\ 0 & 0 & 0 & 0 & 0 & Q_{66} & 0 & 0 & 0 \\ 0 & 0 & 0 & 0 & e_{15} & 0 & \epsilon_{11} & 0 & 0 \\ 0 & 0 & 0 & e_{15} & 0 & 0 & 0 & \epsilon_{11} & 0 \\ e_{31} & e_{31} & e_{33} & 0 & 0 & 0 & 0 & 0 & \epsilon_{33} \end{bmatrix} \begin{bmatrix} \epsilon_{11} \\ \epsilon_{22} \\ \epsilon_{33} \\ \gamma_{23} \\ \gamma_{13} \\ \gamma_{12} \\ E_1 \\ E_2 \\ E_3 \end{bmatrix}; \quad (56)$$

here, the (1,2)-plane is the isotropic plane, and $Q_{66} = (Q_{11} - Q_{12})/2$ holds. The specific material parameters for PZT-5A are given in Tab. 8.

Elasticity moduli [10^9Nm^{-2}]	Q_{11}	Q_{12}	Q_{13}	Q_{33}	Q_{44}
	121	75.4	75.2	111	21.1
Piezoelectric coefficients [Cm^{-2}]	e_{31}	e_{33}	e_{15}		
	- 5.46	15.8	12.32		
Permittivities	ϵ_{11}	ϵ_{33}			
	$1730\epsilon_0$	$1700\epsilon_0$			

Table 8. Material parameters for PZT-5A ($\epsilon_0 = 8.854 \times 10^{-12} \text{AsV}^{-1}\text{m}^{-1}$)

For a uni-axial stress in the 1-direction and for $D_1 = 0$ and $D_2 = 0$, we have $E_1 = 0$, $E_2 = 0$, $\gamma_{12} = 0$, $\gamma_{23} = 0$ and $\gamma_{13} = 0$; moreover, from $\sigma_{22} = \sigma_{33} = 0$ we find the effective constitutive relation as

$$\begin{bmatrix} \sigma_{11} \\ D_3 \end{bmatrix} = \begin{bmatrix} E & -e \\ e & \eta \end{bmatrix} \begin{bmatrix} \epsilon_{11} \\ E_3 \end{bmatrix}, \quad (57)$$

with

$$E = Y(1 - \nu^2), \quad e = \bar{e}(1 - \nu), \quad \eta = \bar{\eta} + \frac{\bar{e}\bar{e}}{Y} \quad (58)$$

and Y , ν , \bar{e} and $\bar{\eta}$ from

$$Y = Q_{11} - \frac{Q_{13}Q_{13}}{Q_{33}}, \quad Y\nu = Q_{12} - \frac{Q_{13}Q_{13}}{Q_{33}}, \quad \bar{e} = e_{31} - \frac{e_{33}Q_{13}}{Q_{33}}, \quad \bar{\eta} = \epsilon_{33} + \frac{e_{33}e_{33}}{Q_{33}}. \quad (59)$$

The density of PZT-5A is $\rho = 7750\text{kgm}^{-3}$. For isotropic aluminum we have $E_{al} = 71 \times 10^9\text{Nm}^{-2}$, $\nu_{al} = 0.33$ and $\rho_{al} = 2700\text{kgm}^{-3}$.

